Anni Henrike Schlüter

Tracking major changes in wildfire regimes during MIS 12 and MIS 16 in the western Iberian Peninsula

UNIVERSIDADE DO ALGARVE

Faculdade de Ciências e Tecnologia

2024

Anni Henrike Schlüter

Tracking major changes in wildfire regimes during MIS 12 and MIS 16 in the western Iberian Peninsula

Master in Coastal and Marine Systems

Supervisor:

Anne-Laure Daniau

Co-supervisor:

Cristina Veiga-Pires

UNIVERSIDADE DO ALGARVE

Faculdade de Ciências e Tecnologia

2024

Acknowledgments

First and foremost, I would like to thank Dr. Anne-Laure Daniau for her mentorship and guidance through this research and for sharing all the ups and downs with me. Her support did not only enable me to conduct this research but also made me feel welcome in the new surroundings of the Hydroshifts project and Bordeaux. Having the chance to work with someone who is that established in her field and also receiving her expertise and constructive criticism during this process were a huge honour and enabled me to develop high-quality research within the project. I am also profoundly grateful to Dr. Cristina Veiga-Pires for guiding me through this process as well as for her unwavering support in helping me achieve the objectives of this research. Additionally, I would like to thank Dr Filipa Naughton who is the reason that I got the chance to be part of this project and supported and believed in me from the beginning and who was always there for me for every question. My sincere gratitude also goes to Muriel Georget who supported all my laboratory work and encouraged me to embrace even the polishing plate as part of the process. Last but not least, I would also like to thank Dr Luis Nunes for helping my statistical skills.

I am also more than grateful to the institutions that played a crucial role in the development of this research: the University of Algarve (UAlg), the Portuguese Institute for Sea and Atmosphere (IPMA) and the Portuguese Foundation for Science and Technology (FCT) for funding my BII scholarship within the Hydroshifts project (PTDC/CTA-CLI/4297/2021).

Dedication

This thesis is dedicated especially to my housemates and friends in Bordeaux, whose love, and unconditional support have made me feel at home here. Without the daily support of loving people reaching these academic goals and experiencing this academic as well as cultural journey would not have been possible.

I also extend my deepest gratitude to all my family and friends who had to share periods of stressful production of a MSc thesis the second year in a row. Thank you for always reminding me of my potential, for supporting me in every decision I have made albeit the senselessness of some.

This accomplishment would not have been possible without each and every one of you.

Abstract

Global warming and a predicted unprecedented increase in CO_2 by 2100 underscore the urgent need for an enhanced understanding of the climate system. Accelerated global warming is impacting ice sheet melting and intensifying climate hazards, particularly in vulnerable regions. Transitional periods between glacial and interglacial states, including glacial terminations, have historically seen rapid temperature and CO_2 increases every 100 kyr, accompanied by abrupt climate shifts occurring over millennial to century scales. The main objective of this master project is to document changes in biomass burning and wildfire regimes during glacial periods (Marine Isotope Stages (MIS) 16 and 12) in the western Iberian Peninsula and explore its relationship with vegetation type and climate conditions obtained in the framework of the Hydroshifts project (PTDC/CTA-CLI/4297/2021). These periods offer a unique opportunity to understand the non-linear behaviour of the climate system, serving as valuable benchmarks for testing the forecasted climate. Through microcharcoal analysis, variations of fire regimes during dry (glacial) was determined and compared with vegetation data, obtained by other researchers in the framework of the Hydroshifts project. The main findings showed that under drier (colder) conditions as modulated by orbital factors and AMOC shut-down during MIS 12 increased fire activity is stronger associated with semi-desert vegetation. During wetter conditions as found in MIS 16 due to higher amplitude of precession and AF position further north, fire activity was lower and more associated with heathland vegetation. Albeit both being strong glacials, these differences in relative wetness can be attributed to the strength of the Atlantic meriodional overturning circulation (AMOC) and its influence on the location of the Arctic Front (AF) which modulates the climate on the western-Iberian Peninsula and leads to different fire activity behaviour.

Key words: Fire regimes, MIS 12, MIS 16, microcharcoal, SW Iberia

Resumo

O aquecimento global e um aumento sem precedentes de CO_2 previsto até 2100 sublinham a necessidade urgente de uma melhor compreensão do sistema climático. O aquecimento global acelerado está a ter impacto no degelo dos glaciares e a intensificar os riscos climáticos, especialmente nas regiões vulneráveis. Os períodos de transição entre estados glaciares e interglaciares, incluindo as terminações glaciares, têm registado historicamente aumentos rápidos de temperatura e de CO_2 a cada 100 kyr, acompanhados por mudanças climáticas abruptas que ocorrem em escalas milenares a centenárias. Assim, o estudo dos estados glaciares que precedem estas rápidas transições, especialmente em regiões vulneráveis às alterações climáticas, é importante para as medidas de adaptação.

O Mediterrâneo, incluindo o sudoeste (SW) da Península Ibérica, é muito suscetível a aumentos na extensão, gravidade e frequência dos eventos de seca provocados pelo aumento da evaporação e pela redução da precipitação (Giorgi e Lionello, 2008). Isto leva a um risco acrescido de incêndios florestais e a danos irreversíveis nos ecossistemas naturais (Ruffault, 2020). Além disso, o aquecimento global está também a contribuir para o degelo dos glaciares do Hemisfério Norte, o que provoca a subida do nível do mar e uma redução da circulação meridional do Oceano Atlântico (AMOC). Uma redução da AMOC provoca um maior contraste de temperatura entre as latitudes elevadas e médias do Atlântico Norte (NA) (Caesar et al., 2018) e, assim, altera a circulação atmosférica, o que, por sua vez, leva ao aumento da ocorrência de eventos climáticos extremos no sudoeste da Europa. As regiões já áridas estão a tornar-se mais secas, com riscos de incêndio consequentemente mais elevados relacionados com épocas de incêndios mais longas, bem como com um aumento na intensidade de outros perigos naturais (JRC, 2014). Em 2017, ocorreu uma série de incêndios florestais que afetaram o oeste da Península Ibérica, queimando cerca de 500.000 hectares de área natural e causando vítimas humanas. Estes eventos foram explicados através de simulações climáticas recentes, pelas temperaturas elevadas e pela persistência da seca estival (Turco et al., 2019).

O principal objetivo do presente projeto de mestrado foi documentar as alterações nos regimes de queima de biomassa e de incêndios florestais durante os períodos glaciares (Estágios Isótopos Marinhos (MIS) 16 e 12) no oeste da Península Ibérica e explorar a sua relação com o tipo de vegetação e as condições climatéricas obtidas neste âmbito. Estes dois períodos oferecem uma oportunidade única para compreender o comportamento não linear do sistema

climático, servindo como referências valiosas para testar o modelo climático considerando as semelhanças e diferenças das respostas climáticas no último período glaciar (Past Interglacials Working Group of PAGES et al., 2016). Através da análise de microcarvão, foram determinadas as variações dos regimes de fogo durante a seca (glaciar) e comparadas com dados de vegetação, obtidos por outros investigadores no âmbito do projeto Hydroshifts.

Para o efeito, foram aplicados critérios petrográficos para identificar e quantificar partículas de microcarvão utilizando uma análise automatizada de imagens num microscópio Leica DMRBE com ampliação de 500x. Um total de 200 imagens de amostras foram analisadas para garantir robustez estatística. A análise de imagem identifica também partículas não queimadas, verificando a ausência de estruturas vegetais e diferenças na reflectância, garantindo a identificação precisa de microcarvão. A partir das medições laboratoriais foram calculados os seguintes parâmetros para cada amostra: Concentração de Microcarvão (CCnb), Concentração de Área Superficial de Microcarvão (CCs), Área Superficial Média e Alongamento (relação comprimento/largura). Os valores de alongamento foram estabelecidos em 2,2 e 1,8 para distinguir entre incêndios em pastagens e matagais. Além disso, as partículas de microcarvão foram classificadas com base nas taxas de alongamento em tipos de árvores e arbustos (alongamento <2,5), arbustos e gramíneas (2,5-3,5) e gramíneas (alongamento >3,5), com percentagens correspondentes calculadas. A análise estatística, incluindo ANOVA, testes HSD de Tukey e testes de correlação de Pearson, foi realizada para comparar a concentração e o alongamento do carvão vegetal entre os tipos de vegetação, utilizando o programa R 4.3.2. Estes testes ajudaram a avaliar a importância dos padrões observados na concentração de carvão e nos regimes de fogo.

O MIS 12, caracterizado por uma Circulação Meridional do Oceano Atlântico (AMOC) enfraquecida e uma posição da Frente Polar Ártica mais a norte e, portanto, por condições mais áridas, registou uma atividade significativa de incêndios, predominantemente alimentada por pastagens e vegetação semidesértica. Os mínimos de precessão durante o MIS 12 contribuíram para verões mais quentes, secando a vegetação e aumentando a frequência e intensidade dos incêndios. A atividade de incêndios durante o MIS 12 pode ser classificada, seguindo Karp et al. (2023), como limitada pela humidade do combustível, onde as condições de seca promoveram a queima de vegetação florestal semidesértica e mediterrânica.

Em contraste, o MIS 16 apresentou um clima mais estável com menos atividade de fogo, impulsionado por uma AMOC relativamente forte e condições mais húmidas que suportaram

uma vegetação lenhosa mais resistente ao fogo. Durante este período, os regimes de fogo foram de carga limitada, com incêndios a ocorrerem durante períodos mais húmidos, quando o aumento do crescimento da vegetação fornecia combustível suficiente, especialmente em ambientes de charneca. Esta dinâmica reflete um sistema de "quantidade de combustível limitada ao fogo excluído" (classificação de Karp et al. (2023)), onde o fogo era mais prevalente em florestas mediterrânicas abertas, mas reduzido em ambientes florestais fechados.

Quando comparado com o Último Período Glaciar, o MIS 16 apresenta semelhanças no comportamento do fogo, com um aumento da atividade de incêndios durante os períodos mais húmidos, enquanto o MIS 12 contrasta ao apresentar uma maior atividade de incêndios durante as fases mais secas e frias. O Último Período Glaciar, com o seu clima mais seco e vegetação semidesértica no sudoeste da Península Ibérica, viu a atividade de incêndios mais estreitamente alinhada com sistemas de carga de combustível limitada, embora menos intensa do que durante o MIS 12. A maior atividade de incêndios durante os estádios frios do MIS 12 destaca uma resposta única às alterações climáticas, impulsionada pelo colapso do AMOC e pelo forçamento orbital.

Este estudo destaca as complexas interações entre o clima, a vegetação e os regimes de incêndios durante os períodos glaciares, ilustrando como fatores externos, como os ciclos da precessão e obliquidade, juntamente com fatores internos, como a AMOC e a circulação atmosférica, moldaram a dinâmica dos incêndios. A comparação com o Último Período Glaciar destaca a variabilidade nas respostas do fogo às alterações climáticas e fornece informações importantes sobre as relações clima-fogo passadas e futuras.

Palavras-chave: Regimes de fogo, MIS 12, MIS 16, microcarvão, Península Ibérica do SO

Table of Contents

Table of Figures

List of Abbreviations

AMOC	Atlantic Meridional Overturning Circulation
ANOVA	Analysis of Variance
CCnb	Concentration of microcharcoal
CCs	Concentration of microcharcoal surface area
crmcd	Corrected Revised Meter Composite Depth
D-O	Dansgaard-Oeschger
FCT	Fundação para a Ciência e a Tecnologia
HE	Heinrich Event
HS	Heinrich Stadial
IPMA	Instituto Português do Mar e da Atmosfera
IODP	International Ocean Discovery Program
IRD	Ice-rafted debris
ITCZ	Intertropical Convergence Zone
Ka	Thousand of years ago
kyr	Thousand of years
LR04 stack	Lisiecki and Raymo, 2005 spans 5.3 Myr and is an average record of 57 globally distributed benthic d18O records
MIS	Marine Isotopic Stage
NA	North Atlantic
NAC	North Atlantic Current
NAO	North Atlantic Oscillation
SD	Standard deviation
SST	Sea Surface Temperature
SW	southwest
T	Termination
Tukey'sHSD	Tukey's Honestly Significant Difference (HSD) test is a statistical method used for multiple comparisons after an Analysis of Variance (ANOVA) test.
YD	Younger Dryas

1. Introduction

The current state of our climate with global warming and unprecedented increase in CO_2 concentration predicted for 2100 urgently calls for improved understanding of the climate system. Being aware of the drivers and contributors of natural disasters is necessary to understand adaptation and mitigation measures (IPCC, 2012). Investigating future climate change impacts is crucial to prepare societies for worst-case climate scenarios and to urge policy makers for new adaptation strategies. Climate simulations predict a virtually total deglaciation pattern in the future (Masson-Delmotte *et al.*, 2013; Past Interglacials Working Group of PAGES *et al.,* 2016).

Every 100 kyr (since the mid-pleistocene transition) rapid surges in temperatures and CO_2 concentrations have been recorded which translate to transitional periods between glacial and interglacial climate states, so-called deglaciations and glacial terminations within them (see Figure 1). These cycles are subject to the astronomical forcing of solar radiation, especially the cycles of precession (23,000 yrs) and obliquity (41,000 yrs). Generally, ice growth in the northern hemisphere happens during low summer insolation (during low obliquity and precession maxima, i.e. when Earth is in the aphelion position). During high obliquity and

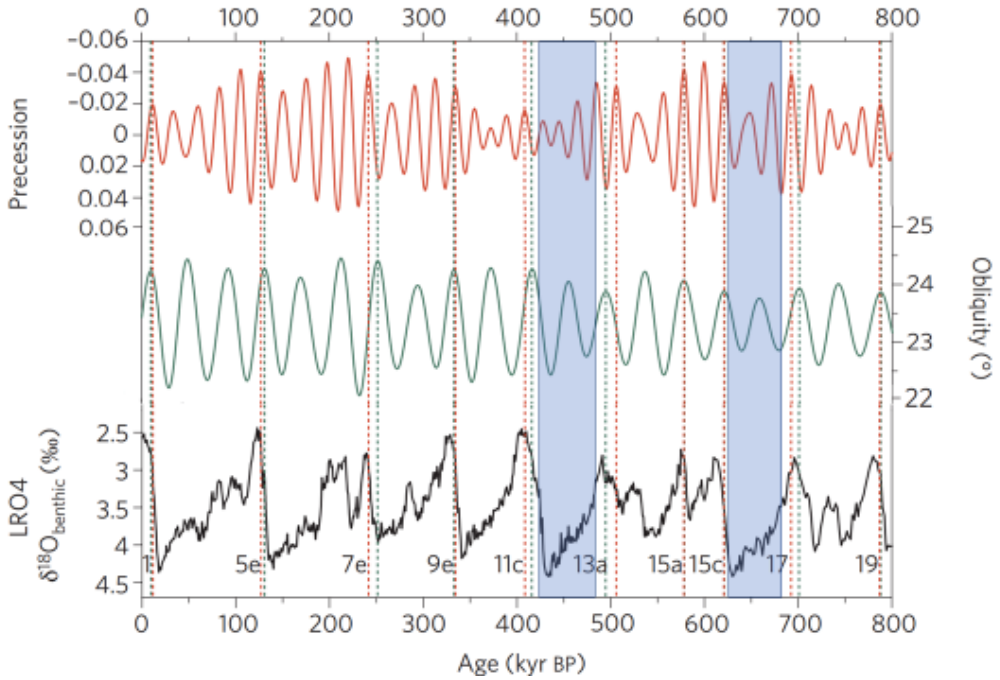

Figure 1 | Palaeoclimate parameters of the past 800 kyr. Precession parameter plotted on an inverse vertical axis. Obliquity. $\delta^{18}O$ benthic record from the LR04 stack11. Marine isotope stages and substages of interglacial status are shown. Vertical dotted lines indicate the timing of precession minima (red) and obliquity maxima (green). Note the similarities and differences to the last termination (dashed line to the left) (Adapted from Tzedakis et al., 2009)

precession minima (Earth in the perihelion position), ice melts. The most sensitive latitude where the ice sheets first accumulate and last melt would be at 65°N (Ruddiman, 2001). However, there are also internal forcing factors such as greenhouse gas emissions and feedback loops.

Glacial periods represent natural fluctuations in Earth's climate. By studying these periods, insights can be gained on how the Earth's climate responds to changes in factors such as atmospheric composition, ocean circulation, and solar radiation. Studying this interaction is essential to understanding the relationship between CO_2 levels, global temperature, and climate feedback mechanisms, which are relevant for current climate change scenarios. For instance, oceanic currents are influenced by glacials through the input of freshwater and temperature differences. Since they are a significant regulator of global climate (e.g. through the carbon cycle) it is of utmost importance to understand how glacial periods impacted them to improve the predictions of future changes. Especially with regards to anthropogenic climate change, these findings are useful to assess the potential consequences of human activities.

Key glacial terminations such as TVII (MIS 16): (~ 625 kyr) and TV (MIS 12): (~ 430 kyr) reveal close similarities with the ongoing global warming such as steep rise in temperatures, CO_2 concentration and sea-level caused by the rapid retreat of ice sheets. In addition to mentioned similarities between the transitions, TV has a similar boundary conditions to TI, whereas TVII, the transitional period between MIS 16 and MIS 15 has dissimilar boundary conditions with a high increase of boreal summer insolation and lower CO_2 concentrations (e.g. Past Interglacials Working Group of PAGES *et al.,* 2016). The character of glacial termination is determined by these boundary conditions which also shape the glacial periods preceding the terminations. In the following study, the focus will lie on the entire glacial periods of MIS 12 and MIS 16 to understand how and why similarities and differences are shaped.

The Mediterranean, including the south western (SW) Iberian Peninsula is very susceptible to increases in extent, severity and frequency of drought events driven by enhanced evaporation and deficient precipitation (Giorgi and Lionello, 2008). This leads to an increased risk of wildfires and irreversible damages of natural ecosystems (Ruffault, 2020). Additionally, global warming is also contributing to the melting of the ice sheets in the Northern Hemisphere, which causes sea level rise, and a reduction of the Atlantic meridional overturning circulation (AMOC). A reduction in AMOC causes a higher contrast in temperature between North Atlantic (NA) high- and mid-latitudes (Caesar *et al.,* 2018) and thus changes the atmospheric circulation, which in turn leads to increased occurrence of extreme weather events over SW

Europe. Already arid regions are becoming drier with corresponding higher fire risks relating to longer fire seasons, as well as an increase in intensity of other natural hazards (JRC, 2014). In the recent past, there has been a series of wildfires that affected western Iberia in 2017, burning ca. 500,000 ha of natural area and causing human casualties. These events were explained by high temperatures and persistence of summer drought by recent climate simulations (Turco *et al.,* 2019). Next to the climatic conditions, the vegetation type influences the occurrence of wildfires. The vegetation type is determined by the prevalent climatic conditions, which change on different time scales varying from inter-annual (vegetation productivity) to multi-millennial (vegetation dynamics and distribution) (Daniau *et al.,* 2019). To study wildfire regimes of the past and thus gain insights potentially applicable to the future, microcharcoal particles in sediments are an indicator for the variability of these fire regimes. Especially marine sediments provide long records of accumulation. For this study, the record discovered on the International Ocean Discovery Program (IODP) expedition 339 at site U1385 was analysed. The strength of the Portuguese margin sediment record is the ability to correlate millennial-scale climate events from the marine environment to polar ice cores in both hemispheres. Moreover, the narrow continental shelf and proximity of the Tagus River result in rapid delivery of terrestrial material to the deep-sea environment off Portugal, thereby providing a record of vegetation changes and permitting correlation of marine and ice-core records to European terrestrial sequences (Stow *et al.,* 2013). There have been various studies on the same location and core (cf. PANGAEA).

1.1. Objectives

The main objective of this study is to document changes in biomass burning and wildfire regimes during glacial periods MIS 16 and MIS 12 in the western Iberian Peninsula and explore its relationship with vegetation type and climate conditions (both temperature and precipitation) obtained in the framework of the Hydroshifts project (PTDC/CTA-CLI/4297/2021).

The Hydroshift project focuses on the improvement of comprehending the dynamics of the climate system and abrupt climate shifts especially where affecting hydroclimate regimes in regions vulnerable to ongoing global warming as is the case of the Mediterranean region in southwest Europe and the south east coast of the USA which are both more exposed to natural hazards such as droughts, storms, wildfires and floods. The research is focused on exploring

the last deglaciation including key glacial terminations (TI: ~ 18 kyr, Denton *et al.,* 2010; TV: ~ 430 kyr and TVII: ~ 625 kyr) as they have similarities with the current warming, e.g. the temperature rise, CO_2 concentration rise and sea-level rise due to the ice sheets retreat. Other factors depending on which termination are dissimilar or similar such as astronomical configuration, levels of greenhouse gases (GHG) concentration and ice volume extent. Notably, termination V is very comparable to TI in terms of astronomical configuration with less insolation over the earth during boreal summer related to low eccentricity and thus weak precession (e.g. Past Interglacials Working Group of PAGES *et al.,* 2016). On the other hand, TVII (between MIS 16 and MIS 15) is dissimilar in boundary conditions to TV and TI with a higher increase in boreal summer insolation but less CO_2 concentrations (e.g. Past Interglacials Working Group of PAGES *et al.,* 2016). All of the mentioned glacial terminations have distinct patterns of millennial scale variability marked by baseline conditions that define the preceding glacial stage (e.g. Past Interglacials Working Group of PAGES *et al.* 2016). Hence, the Hydroshifts project provides trial cases to test critical modes of paleoclimate dynamics to test the role of orbital parameters (external factors) and internal forcing factors such as ice sheet extent, GHGs etc. on the generation and modulation of abrupt millennial-scale variability

1.2. State of the art

Although there are abundant regional records providing detailed temporal information for the Last Termination (TI), the same cannot be said for older glacial terminations. Many existing records lack the necessary chronological precision and resolution to identify abrupt climate shifts. Furthermore, despite TI being extensively studied, the factors influencing abrupt climate instabilities, particularly hydroclimate shifts in Southwest Europe, remain poorly understood. Notably, extreme cold episodes during the last deglaciation (Heinrich Stadial 1-HS1 and Younger Dryas-YD) had different triggers (e.g., Denton *et al.,* 2010; Renssen *et al.,* 2015) but led to anomalous freshwater input in the North Atlantic, causing a slowdown in the Atlantic Meridional Overturning Circulation (AMOC) (e.g. Shakun and Carlson, 2010; Ng *et al.,* 2018). While model simulations suggest persistent dry conditions in Western Europe and Eastern USA due to these perturbations (Ganopolski and Rahmstorf, 2001), paleo-observations reveal a more complex hydroclimate signal in the North Atlantic mid-latitudes. These observations indicate phases of extreme wetness that cannot be solely attributed to AMOC slowdown, necessitating consideration of atmospheric mechanisms (e.g. Renssen and Isarin, 1997; Brauer *et al.,* 2008; Naughton *et al.,* 2009; 2016; 2019). Various studies emphasize that a comprehensive understanding requires high-quality data from multiple locations to capture temporal and spatial

variability for regional comparisons with model outputs (Naughton *et al.,* 2009; 2016; 2019). Consequently, the Hydroshifts project aims to address these gaps by conducting high-resolution sea-land comparisons using pollen, microcharcoal, and terrestrial and marine biomarkers on marine cores from Southwest Europe, Southeast USA, and high latitudes of the North Atlantic, spanning crucial glacial terminations.

Previous studies on marine cores from the Southern Hemisphere have established a connection between fire history and orbital-scale climatic variability over Glacial/Interglacial cycles (Verardo and Ruddiman, 1996; Bird and Cali, 1998; Kershaw *et al.,* 2002; Beaufort *et al.,* 2003; Thevenon *et al.,* 2004). Today, fires are observed in both hemispheric regions throughout the year, impacting the atmosphere's chemistry with the release of radiative and chemically active gases, including greenhouse gases (carbon dioxide, methane, nitric oxide) and particulates (Crutzen *et al.,* 1979; Lobert *et al.,* 1990; Carmona-Moreno *et al.,* 2005; Thonicke *et al.,* 2005). Biomass burning is recognised as a small but significant driver of climate change (Arneth *et al.,* 2010; Clark *et al.,* 1997) with current CO_2 emissions equal to 50 % of those coming from fossil-fuel combustion (2 to 4 Pg C $year^{-1}$ versus 7.2 Pg C $year^{-1}$) (Bowman et al., 2009). Shifts in fire regime emissions between D–O interstadial and stadial periods in the past could have contributed to variations in atmospheric greenhouse gas concentrations identified in Greenland and Antarctic ice cores during the last climatic cycle (Daniau *et al.,* 2007). Thus, studying the fire regime in the past provides insights into changes in atmospheric conditions and facilitates discussions on feedback mechanisms through fire-derived greenhouse gases (Harrison & Goñi, 2010). Charcoal particles, as intermediates between vegetation debris and soot, exhibit resistance to chemical and microbial decomposition and are thus a proxy to fire regimes. There is no significant time lag between the production and deposition of microcharcoal in marine records as the resolution is normally not precise enough to monitor centennial time lags. If there is time lag, it is likely within the error of the dating (Daniau *et al.,* 2007).

Paleoenvironmental records in Western Europe, detailing paleofires extending back to the Last Interglacial, have been rare. A study of microcharcoal particles preserved in marine core MD95-2042, retrieved off southwestern Iberia, covering the last climatic cycle showed that fire emissions are predominantly influenced by the 23,000-year precessional cycle (Daniau *et al.,* 2007). The fire activity in southwestern Iberia preserves also a strong imprint of Dansgaard–Oeschger (D–O) oscillations and Heinrich Events (HE) (Daniau *et al.* 2007). D–O stadials are marked by a decrease in sea surface temperature and heavy planktonic oxygen isotopic values (Shackleton *et al.,* 2000a, b), while D–O interstadials exhibit warmer sea surface temperatures

and lighter planktonic isotopic values. Lowest fire activity corresponds to D-O stadials and HE, with the D–O climatic variability significantly impacting the region's vegetation (Cayre *et al.,* 1999; Gendreau, 1999; Sánchez Goñi *et al.,* 2002; Sánchez Goñi, 2006). The study suggests that during D–O stadials, a prevailing south-easterly wind component, similar to contemporary observations during large wildfires in Portugal (Pereira *et al.,* 2005), was enhanced and more frequent due to a positive North Atlantic Oscillation (NAO)-like situation. Evidence for a breakdown in upwelling activity during D–O stadials on the Portuguese margin further supports a dominant southeasterly wind (Daniau *et al.,* 2007). During HE and D–O stadials, fires are inferred to propagate in semi-desert vegetation, resulting in low microcharcoal quantities. In contrast, during interstadials, fires in the Mediterranean forest and heathland lead to higher microcharcoal input, reflecting changes in biomass availability accompanying millennial-scale climatic variability (Daniau *et al.,* 2007).

The fire regime in southwestern Iberia appears to be indirectly controlled by climatic variability. Periods characterised by major drought (D–O stadials) exhibit low fire activity due to weak biomass availability in semi-desert vegetation which can be found in low quantity of microcharcoal and larger elongated particles. In grassland environments the fire residence time and intensity is usually low, hence bigger particles can be produced. In contrast, warmer and wetter interstadials are associated with increased fire activity and intensity due to higher fuel availability from the spread of the Mediterranean forest and heathland which results in smaller, wider particles (rather square-shaped) (Daniau *et al.,* 2007). This sort of fire is consistent with vegetation reconstruction from pollen analysis and in addition, modern fires have shown very high charcoal concentrations and small particles produced by heathland vegetation (Blackford, 2000).

Additionally, there have been studies located in other areas and climatic regimes such as South Africa, which findings notably differ or complement to the ones from southwestern Iberian Peninsula. A strong correlation was found between the amplitude of biomass burning in Southern Africa and the magnitude of precession changes with high fire activity during precession maxima and high northern hemispheric ice volumes (Daniau *et al.,* 2012). For instance, the study of Daniau *et al.* (2012) concludes that the mean elongation of microcharcoal particles is an indicator for low-intensity fires spreading in grass-dominated areas. After revision of said study, it is stated that a higher mean elongation reflects grass and shrubs burning and high intensity fires in Southern Africa (Daniau *et al.,* 2023). Here, high fire activity occurs

during maxima of precession and obliquity leading to increases in precipitation (increase in fuel availability) and increase in seasonality (increase in fuel flammability; Daniau *et al.,* 2023).

1.2.1. MIS 16 and 12

MIS 16 and MIS 12 both portray important similarities and dissimilarities to the Last Glacial Period, thus making them valuable research opportunities. Researchers agree on the vast extent of the ice sheet volume, however, there are discrepancies whether there was complete/partial/no shut-down of the AMOC. During the intensification of northern hemisphere glaciations, the North Atlantic current (NAC) is assumed to have a purely west to east flow due to the position change of the arctic front. This leads to increased cooling in the arctic areas as there is less heat transport northwards resulting in bigger ice sheets and an increased meridional Sea Surface Temperature (SST) gradient further intensifying northern hemisphere glaciations (Naafs *et al.,* 2010). During both glacial initiations there was high insolation, however the sea ice growth is thought to have started already earlier during low insolation. The arctic front position changed before and after both glacials (Alonso Garcia *et al.,* 2011), which might have caused slower deep water currents between MIS 15-12 (Head and Gibbard, 2005).

MIS 16 generated the first large ice sheet of the Mid-Late Pleistocene due to low CO_2 levels in phase with Northern Hemisphere climate change, the higher transfer of water vapour, the exposure of the bedrock in Laurentia and the enlargement of climatic cycles (Alonso Garcia, 2011a) which caused the AF to be positioned at 50°N (Rodrigues *et al.,* 2017). Prior to MIS 16 there was no proof of Ice-Rafted Debris (IRD) residues originating from the Laurentide ice sheets which is an indicator for Heinrich Events, making thus MIS 16 the first glacial with their occurrence (Naafs *et al.,* 2013). IRD events are generally linked to ice sheet instability and rapid climate changes (Naafs *et al.,* 2013a). Generally, HEs coincide with periods of CO_2 rise which, because of the interhemispheric seesaw, means simultaneous CO_2 release in the southern hemisphere. Additionally, there is a North Atlantic seesaw pattern in SST during HEs between cold north Atlantic waters and mid-latitude waters. During HEs, there is an increase in wind stress leading to an expansion of the subtropical gyre northwards (northern boundary current intensifies) and simultaneously weakening of the subpolar gyre as the ice expands southwards which is supported by a slow-down of the AMOC (Naafs *et al.,* 2013b). However, there was no fresh water input from the first HE-like events at site U1385 meaning that the IRD did not reach that site (Rodrigues *et al.,* 2017). This leads to the interpretation that MIS 16 surpassed a critical threshold allowing massive surges influencing the Atlantic ice-rafted debris (IRD) belt. Yet, the SSTs in the North Atlantic region were relatively high due to a potential shift in surface

water circulation and arctic front position. The SSTs probably increased due to stronger stratification and thus a lower subsurface temperature (Naafs, 2011). During MIS 16, the North Atlantic overturning circulation was greater than during other glacials, which is related to the relatively high SST. Usually, it has been found that there is a correlation between HEs (in relation to AMOC shutdowns) and warmer interglacials. However, MIS 16 is an exception which might be related to the persistence of the NA overturning potentially indicating, that the HEs were not cold and persistent enough to cause an AMOC shut-down and thus not influencing the succeeding interglacial as much (Naafs, 2011). Controversially, some authors consider MIS 16 as one of the periods with the longest shutdown of AMOC while other authors (cf. Naafs *et al.,* 2013) associate the longest AMOC shut-down with MIS 12. Generally, the longest shutdowns take place at terminations, which causes major reorganisation of ocean and atmosphere, e.g. southern-ocean ventilation increase and CO_2 release. After MIS 16 being the first MIS with a major ice sheet extension, the glacial cycles were mostly obliquity-forced because the large Antarctic ice sheets cancel the precession influence on global sea level change (Alonso-Garcia *et al.,* 2011).

MIS 12 has a similar ice sheet extension to MIS 16. Yet, it displayed lower SSTs. These were the lowest SSTs of the last 3.5 Ma at site U313 (located in the NA at 41°N, 35.57 °W) and thus, MIS 12 can be considered the most severe glacial of the Quaternary (Naafs *et al.*, 2014). This glacial period had a pronounced D-O imprint, which also influenced the SSTs in midlatitude northern Atlantic (Naafs *et al*., 2014). This is noteworthy as D-O oscillations and SST were decoupled during the last glacial (Naafs *et al.,* 2014), showing one of the differences between different glacials even under comparable boundary conditions.

Due to the location further south of the artic front (compared to other glacials), the influence of polar waters was the most significant during MIS 12 (Koutsodendris *et al.,* 2019) which led to a reduction of the north Atlantic current (Naafs *et al.,* 2014). During the interglacial MIS 11 just following MIS 12, the climate started to be highly influenced by obliquity. The Inter-Tropical Convergence Zone (ITCZ) migrated near the equator (Alonso Garcia, 2010). The interglacial MIS 11 was extreme in terms of least amount of ice (Mc Manus *et al.,* 2020), which confirms the correlation between HEs, AMOC and strong interglacials (cf. above).

1.3. Environmental setting

1.3.1. Present-day fires, vegetation and climate

The southwest Iberian Peninsula is characterised by a Mediterranean climate consisting of mild winters and hot, dry summers (Lionello, 2012). The region features Mediterranean forests dominated by evergreen oaks, such as cork and holm oak. Scrublands, including maquis and garrigue, are characterised by plants adapted to dry conditions. Open grasslands with annual grasses are common in arid areas, while riparian vegetation is located along rivers. Human impact, however has significantly altered the landscape through urbanisation and agriculture (Loidi, 2017). Winds are western with a strong north and northwestern component during the summer months resulting from the intensification of Portuguese trade winds and thus the seasonal upwelling from July until September (Lionello, 2012). Currently wildfires are occurring in the dry season, particularly in long, intense dry periods without precipitation in late spring and early summer (Turco *et al.,* 2019).

1.3.2. Microcharcoal production and deposition

Large fires can be characterised by large convection columns consisting out of smoke particles of various sizes. These smoke particles include microcharcoal particles that are transported and later deposited by aeolian and fluvial processes, into sedimentation basins (Whitlock, 2001).

The sizes of the particles can vary from a submicron to several centimetres (Conedera *et al.*, 2009). Generally, particles can travel over long distances (100s km) by low atmospheric winds. However, most particles are subject to fluvial processes through rivers and estuaries and potentially canyons that add particles to marine sedimentation basins in the deep ocean. In water, e.g. in marine sedimentation basins, the particles break down into somewhat rounded particles that eventually become waterlogged and sink to the oceanic floor which can take years. Microcharcoals found in these basins are produced within their hydrographic basin (Haliuc *et al.,* 2023), thus the charcoal particles recovered from the IODP core at location U1385 (cf. Fig. 2) is a proxy for fire from southwest Iberia. Albeit their might be a slight time lag from combustion to sedimentation, Daniau *et al.* (2007) have concluded that this time lag can be disregarded when looking at geological timescale.

2. Materials and Methods

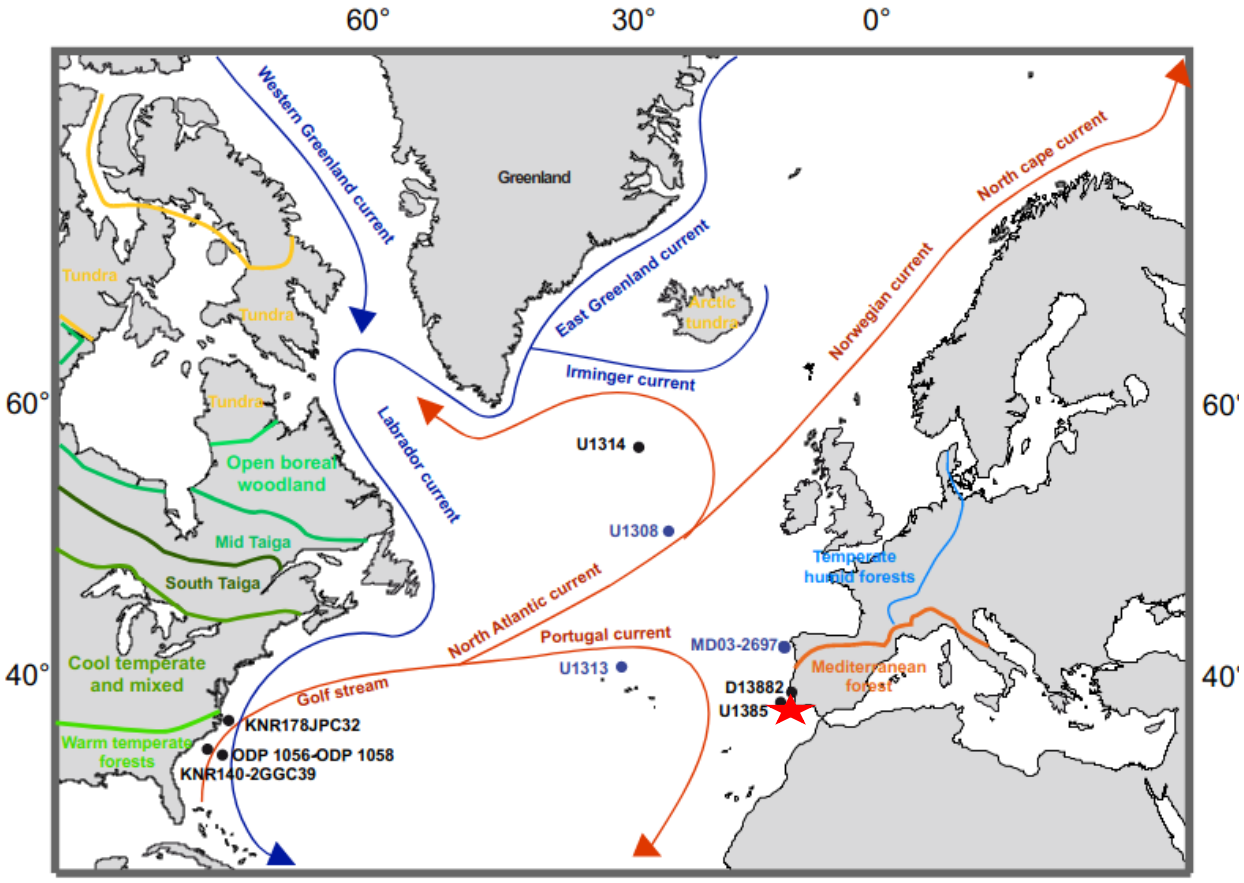

Figure 2 Map of locations within the Hydroshifts project. Note the location of U1385 (the star icon), the sample location for this dissertation (adapted from Naafs et al., 2013)

2.1. Core location, sampling and chronostratigraphy

The IODP Site U1385 (37°34.285′N, 10°7.562′W) coincides with the position of Core MD01-2444, which has been extensively studied. The depth at the sampling site is 2578 m below sea level (mbsl) and therefore is influenced by the Northeast Atlantic Deep Water today, but also by southern-sourced water masses during glacial periods. The core was obtained with nonmagnetic core barrels. Lithostratigraphic analyses have shown the presence of pyrite, dolomite (low abundance), quartz, calcite, feldspar, plagioclase, and clay minerals such as chlorite, illite, and kaolinite (Stow *et al.,* 2013).

Oxygen and carbon isotope measurements in planktic and benthic foraminifera from Site U1385 were made at an average temporal resolution of ~200 years for the last 1.45 million years. The $\delta^{18}O$ benthic curve established from the samples resembles the temperature record from Antarctica, both in shape (the "triangular" form of Antarctic Isotope Maxima) and phasing

relative to Greenland and North Atlantic surface temperature records. This Antarctic affinity largely reflects changes in local deepwater ($\delta^{18}O_{dw}$), which may be due to changes in deep water sourcing and/or source signature. For the microscopic charcoal analysis, 205 samples were analysed with an average spacing of 4 cm (see Annex 3 and 4).

The age model used was developed using the control points of Hodell *et al.* (2023). The chronology is a hybrid model constructed using a combination of age depth points from MD01-2444 and U1385. The age model is accurate to a precession cycle (~23 kyrs) but cannot provide exact absolute or relative dates for millennial events. This shortcoming limits the reliability and estimation of recurrence times of millennial events (Hodell *et al.,* 2023). Our fire regime record covers the period between 418.78 – 480.39 ka and 623.9 – 681.16 ka with a mean temporal resolution of 570 years between samples for MIS 12 and 600 years for MIS 16 with an average spacing of 4 cm.

2.2. Microcharcoal analyses

To achieve and fulfil the objectives the following methods are employed.

The microcharcoal preparation technique, quantification and morphological analysis followed Daniau *et al.* (2019). This was done by concentrating microcharcoal through chemical treatments together with the polished slides technique, which enables the particle observation in transmitted and reflected light. The concentration was done by removing carbonates, silicates, pyrites, humic material, and labile or less refractory organic matter. The organic matter was bleached, thus the microcharcoal particles can be distinguished better from unburned plant material. The chemical treatment included several chemical attacks by adding hydrochloric acid (HCl), followed by cold nitric acid (HNO_3) and hydrogen peroxide (H_2O_2) on approximately 0.2 g of dried bulk sediment. Furthermore, a hydrofluoric acid (HF) addition was employed which was followed by rinsing with HCl to remove colloidal SiO_2 and silicofluorides formed during the HF digestion. The residue was then diluted with a factor of 0.1 which resulted in a suspension filtered onto a membrane of 0.45 µm porosity. A part of this membrane was mounted onto a slide before hand-polishing for microscopic observation.

2.3. Image analyses for microcharcoal counting

Petrographic criteria were used to identify the particles and afterwards quantify them using an automated image analyses on a Leica DMRBE microscope in transmitted light at x500

magnification (LAS software). For robust statistical representation of all samples 200 view-fields were analysed. The image analysis incorporated also the identification of unburned particles, characterised by the absence of plant structures and distinct level of reflectance to ensure correct identification of microcharcoal particles. From the measurements in the laboratory, the following parameters were calculated for each sample:

(a) the concentration of microcharcoal (CCnb), representing the number of fragments per gram ($nb.g^{-1}$);
(b) the concentration of microcharcoal surface area (CCs), which is the sum of all surface areas of microcharcoal in one sample per gram ($mm^2 \cdot g^{-1}$) (using CCs avoids the overrepresentation of CCnb as the result of potential fragmentation during particle production or transport);
(c) the mean microcharcoal surface area per sample (CCs divided by CCnb, μm^2) in order to estimate the intensity of fires (fires of high or low temperature);
(d) the elongation of microcharcoal particles (length/width ratio) to estimate the type of burnt vegetation (forest versus grass-dominated land);

A threshold >10 µm on the particle length was set to ensure the correct identification of microcharcoal instead of minerals or organic matter. The presence of minerals and organic matter, despite the chemical treatments, makes the analysis difficult as they can have very similar shapes and colour, and the automated image analysis often cannot distinguish between the particles. For instance in figure 3, a mineral particle is visible but it would be interpreted as microcharcoal based on shape and colour. Yet, when looking at it with reflected light, one can see that it is a mineral, as it appears brighter than microcharcoal particles. Organic matter on the other hand would not reflect any light and thus not appear in the second picture.

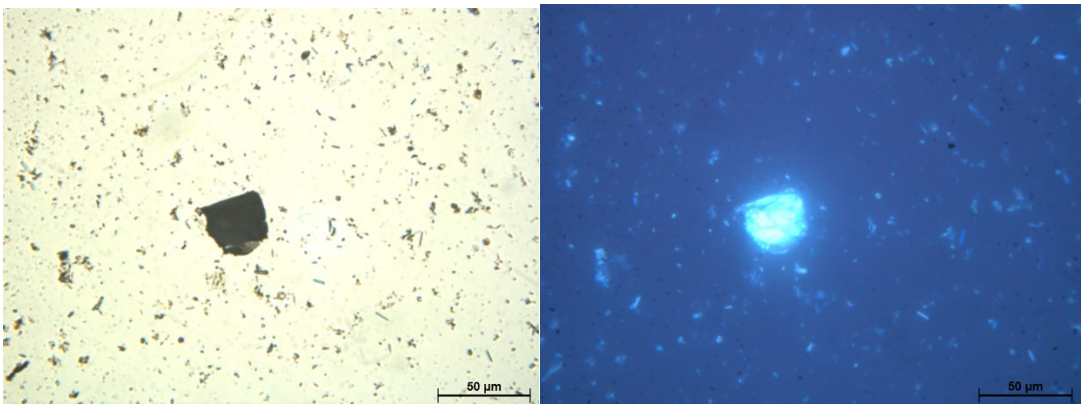

Figure 3 Image of a mineral during the automated image analysis: left: under transmitted light and right: under reflected light.

In contrast, figure 4 shows a charcoal particle from the same series, which reflects much less than the mineral particles in the previous image. Thus, it was opted for employing additional image analysis steps through the use of codes developed by Akabane *et al.* (unpublished) that analysed the same image within both reflected and transmitted light and then compared the texture of the particles to minimise errors of misrecognition.

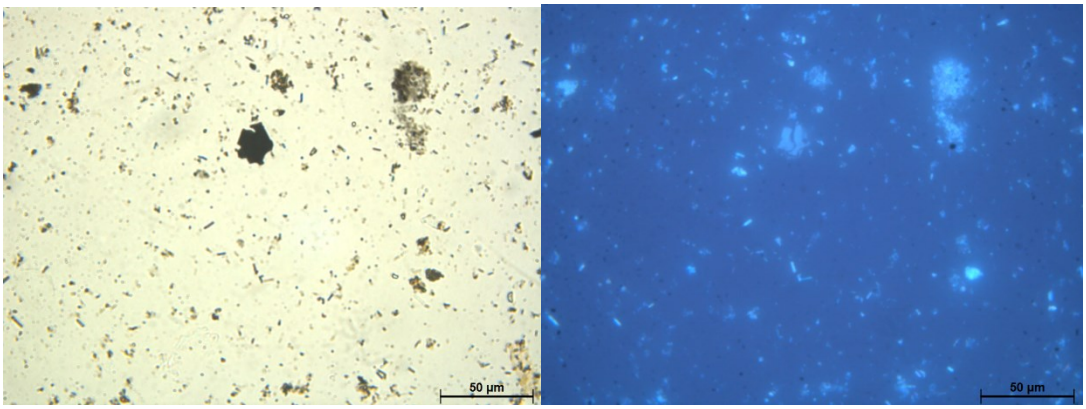

Figure 4 Image of a charcoal particle: left: under transmitted light and right: under reflected light

2.4. Particle classification

Umbanhowar and McGrath (1998) have shown that the elongation degree can be a good indicator for the determination of the burnt vegetation type as charcoal fragmentation occurs along axes derived from plant structures and thus, the elongation degree is preserved even when the particle is broken. Experimentally demonstrated, a morphology with a length/width ratio of one (square-shaped) characterises particles produced during the burning of deciduous forest. This ratio has been used in the geological record to identify shifts in burnt vegetation type. A high ratio (elongated particles) identifies the burning of herbaceous vegetation during the last glacial period while a lower elongation ratio identifies tree burning (Daniau *et al.,* 2007). The mean surface area per sample was used also to estimate the intensity (temperature) of fires

where large mean surface areas correspond to low intensity fires and vice versa (Daniau *et al.,* 2007).

Elongation values above 2.2 following the median value of Haliuc *et al.* (2023) identify charcoal produced by open-grassland savanna fires versus dwarf open shrubland with scattered trees fires following criteria of Leys *et al.* (2015) and Aleman *et al.* (2013) established for Southern Africa. Values above 1.8, following the criteria established by Genet & Daniau (personal communication) for the Mediterranean region, determine the distinction between burnt grassland versus burnt shrub and tree vegetation.

In addition, mean elongation ratios obtained from a synthesis of different experimental analyses conducted on different fuel types (Vachula *et al.,* 2021) were used for further particle classifications. Each individual microcharcoal particle that was detected during analysis was classified as burnt trees and (sub)shrubs (elongation <2.5), shrubs and graminoid (elongation 2.5-3.5) and graminoid only (elongation >3.5). Percentages of burnt trees and (sub)shrubs, shrub/graminoid, and graminoid vegetation were then calculated.

2.5. Statistical analysis

In addition to the graphical inspection of the developed curves a statistical analysis in R 4.3.2. was performed. The analysis was conducted using Analyses of Variance (ANOVA) and post-hoc Tukey's Honestly Significant Difference (HSD) tests from the char package in R to compare the charcoal concentration and elongation across the different dominating vegetation types. Additionally, a Welch's ANOVA test, also from the {stats} package, was used to account for unequal variances across groups (see Annex 1.1., 1.2.). These tests were performed using the R Commander interface for ease of use. Additional correlation tests (Pearson correlation test, see Annex 1.3.) were applied when no statistical significance was found. Boxplots and paired t-tests were employed to compare pollen percentages across glacials (see Annex 2.).

3. Results

3.1 Charcoal concentration and morphology

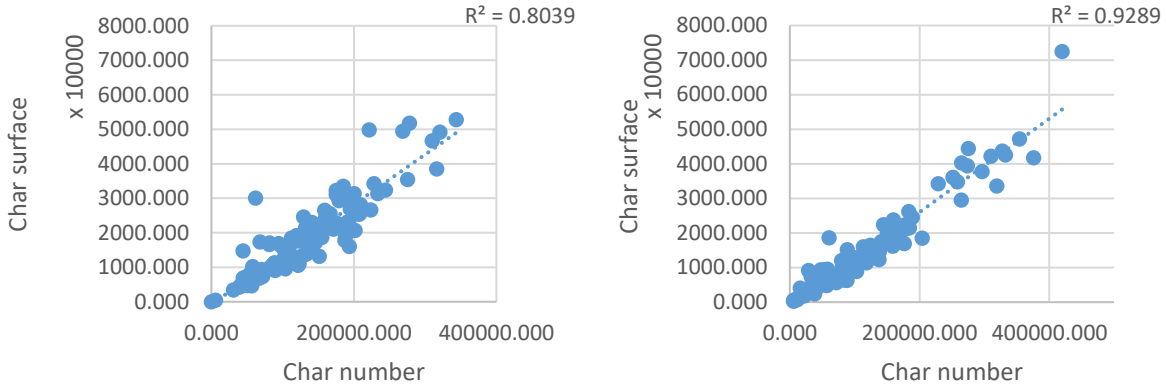

Figure 5 Char number (nb.g^{-1}) plotted against Char surface (µm².g^{-1}) to show correlation between the two variables. The R^2 value is given in the upper right corner. Left: values for MIS 12. Right: values for MIS 16.

The analyses have shown that microcharcoal concentrations (CCnb) and surface (CCs) are highly correlated (Fig. 5, r = 0.964 for MIS 16 and 0.897 for MIS 12 P< < 0.001)), which signifies that there is no noteworthy fragmentation bias when using only Charcoal concentration for interpretation as a proxy of fire activity. Charcoal concentration appears to be highly variable over the record, particularly during MIS 16 marked by large changes in amplitude. Significant maxima (grey bars) were marked by visual inspection of distinct Charcoal concentration peaks after averaging the curve with a window of 5. The weighted average was chosen to make the curves more readable. The peaks for the Charcoal concentration curve of MIS 16 were defined by choosing the bigger (more significant peaks) or when there was a trend of three subsequent peaks resulting in a more noticeable peak. The Charcoal concentration shows an oscillating curve for both glacials with 10 maxima for MIS 12 (418-482 ka) at approximately 434, 439, 442, 449, 452, 453.5, 459, 465, 469, and 478 ka (Fig. 6 and 7, grey bars). Five peaks were defined for MIS 16 (624-683ka) at approximately 636, 650, 666, 671, and 679 ka (Fig. 6 and 8, grey bars). Charcoal concentration are globally higher during MIS 12 compared to MIS 16.

Charcoal morphology classification using different elongation thresholds (Fig. 8) suggests that the burnt particles were produced by both ligneous and grassy vegetation burning over both glacials.

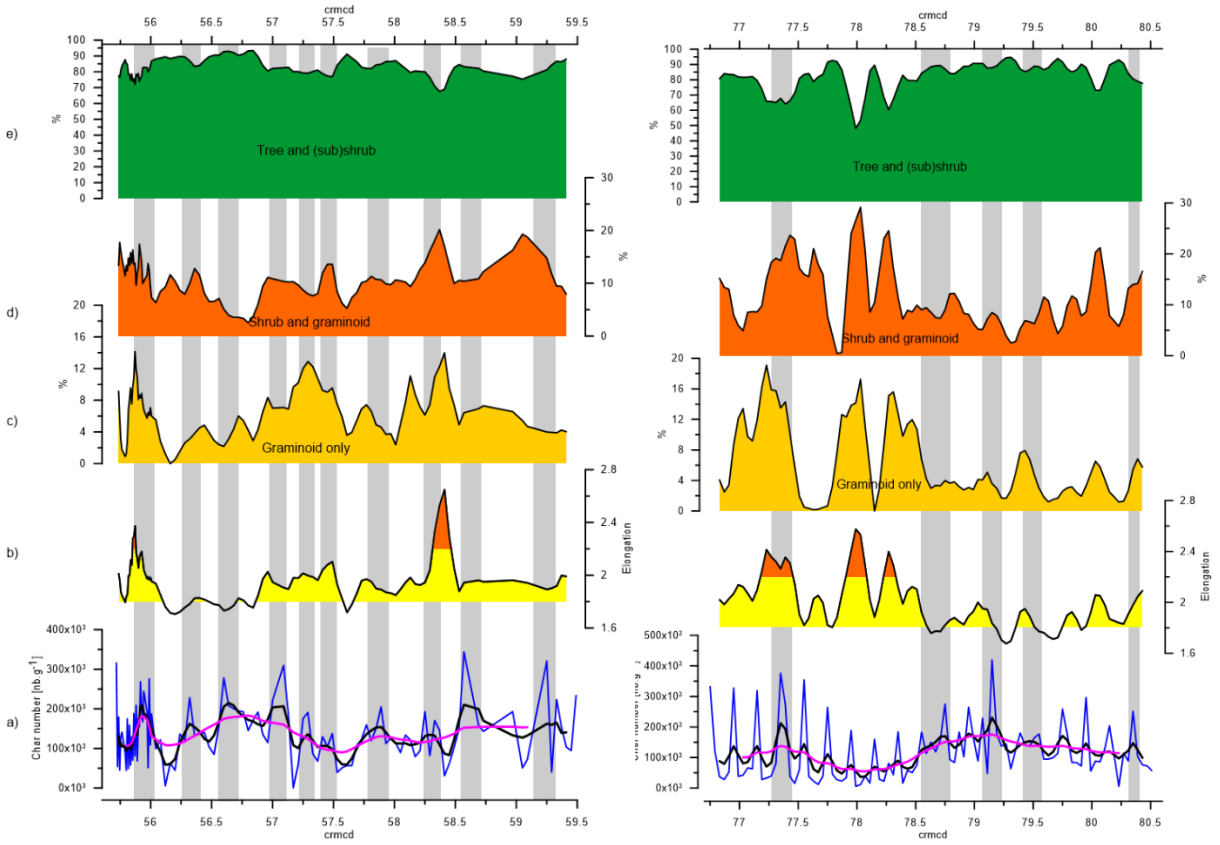

Figure 6 Microscopic charcoal particles retrieved from core IODP Site U1385 along core depth (crmcd) (MIS 12 to the left, MIS 16 to the right). a) Microcharcoal concentration (CCnb) of core IODP U1385 with a weighted curve (black line) with a window of 5 and a weighted curve (pink line) with a window of 15, b) Mean charcoal elongation value of core IODP U1385. Microcharcoal were classified in different burned group based on morphology criteria following b) Haliuc et al. (2023), Aleman et al. (2013), Leys et al. (2015) and c-e) Vachula et al. (2021). Orange colour indicates values above 2.2 following the median value of Haliuc et al. (2023) to identify charcoal produced by open-grassland savanna fires versus dwarf open shrubland with scattered trees fires. This threshold is similar to the one used by Leys et al. (2015a) and Aleman et al. (2013) (width/length of 0.5 corresponding to a length/width of 2). Yellow colour indicates values above 1.8 determined for distinction between grassland and shrub-tree vegetation (Genet, Daniau, personal communication); c) d) and e) microcharcoal percentages of core IODP U1385 by burnt type categories using criteria of Vachula et al. (2021): c) graminoid only, b) shrub and graminoid, and e) tree and (sub)shrub. A weighted average curve using a window width of 5 was fitted to the data. Grey shaded bars indicate peaks in microcharcoal concentration.

For MIS 12 the mean elongation curve shows peaks at ca. 56, 57, 57.25, 57.5 and 58.25 m (crmcd). All of them lie above the threshold established by Genet & Daniau (pers. com) (1.8, yellow indication in the mean elongation curve of Fig. 6), which would classify the burnt particles as grassland. However, taking the threshold established by Haliuc *et al.* (2023) (2.2, orange indication in the mean elongation curve of Fig. 6), only the peaks at 56 and 58.25m would be produced by grassland. These two peaks are associated with peaks in graminoids/shrub and graminoids and troughs in tree and (sub)shrub. These also relate to peaks in charcoal whereby not all charcoal peaks align with elongation peaks.

For MIS 16 the mean elongation curve shows 3 distinguishable peaks at 77.75, 78.25 and 78.75 m. The curve in general displays several other peaks, which are not as remarkable as the general

curve shows a “zig-zag” pattern. Again, all of the peaks pass the threshold from Genet *et al.* (unpublished) (1.8) but only the three distinguished peaks pass the threshold from Haliuc et al (2023). Only the peak at 77.75 m (crmcd) associates with a peak in charcoal. Again, peaks in graminoids and shrub and graminoids relate to troughs in trees and (subs)shrubs. Peaks in microcharcoal concentration are generally associated with grassland and shrubland charcoal particles, whereas lower microcharcoal concentrations (troughs) take place simultaneous to a slight increase in burnt ligneous particle percentages relative to grassland and shrubland charcoal particles percentages.

3.2 Comparison between charcoal, vegetation, orbital parameters and IRD deposits for MIS12

General trends for MIS 12 (Fig. 7) show that the Mediterranean forest decreases in percentage over the time of the glacial, heathland stays constant, and semi-desert as well as Poaceae increase with temperature decrease. The charcoal concentration oscillates (cf. pink line Fig. 7), yet over the time of the glacial there seems to be no general long-term trend of increase or decrease as opposed to the pollen data (Naughton, unpublished). Highest charcoal concentrations were found during increases of solar radiation (cf. Fig. 7: 443 – 450ka and 465 – 470 ka). There is no clear association visible between the mean elongation curve and the pollen data; however, the coloured thresholds show some positive relation between the elongation degree and heathland. Mediterranean forest seems to follow the general trend of precession in terms of amplitude changes.

Charcoal concentration is peaking with semi-desert vegetation in 8 of 10 peaks, (when additionally including increases of the curves there is an association in 9/10 peaks). Charcoal concentration peaks are associated with several peaks in the Zr/Sr ratio indicating the occurrence of very cold events like the glacial maximum at 442 ka (Tzedakis *et al.,* 2012). This maximum is visible in Fig.7 with the minimum sea surface temperature (7.5°C) during MIS 12 which is displayed in a spike of Zr/Sr ratio and translates into a charcoal peak and a peak in semi-desert, additionally. Furthermore, charcoal concentration peaks occur together with heathland peaks in 2/10 peaks, with Poaceae in 4/10 peaks and with Mediterranean forest in 6/10 peaks. A one-way ANOVA (see Annex 1.1) was conducted to test for differences in mean charcoal concentration across the dominating vegetation (heathland, Mediterranean forest,

semi-desert) to examine the impact of different vegetation (or climate) types on charcoal number. Poaceae was not included as it was never the dominating vegetation. The ANOVA results revealed a significant effect of vegetation type (climate) on charcoal concentration with an F value of 10.49 and a p-value of 0.00008. This indicates that there are statistically significant differences in charcoal concentration between the climate groups. To identify where these differences occur, a post-hoc Tukey's HSD test was performed. The results showed that both Mediterranean forest and semi-desert had significantly higher charcoal concentration compared to heathland. These results were supported by a Welch test, which accounts for unequal variances. The Welch test produced similar results, with a significant F value of 10.897 and a p-value of 0.00038, confirming that the differences between the climate groups are robust. Specifically, the mean charcoal concentration in Mediterranean forest was 67,120 units higher than in heathland ($p = 0.00323$), and the mean charcoal concentration in semi-desert was 52,765 units higher than in heathland ($p < 0.001$). However, there was no significant difference in charcoal concentration between Mediterranean forest and semi-desert ($p = 0.739$). Peaks are associated with semi-desert and Mediterranean forest, a high Zr/Sr ratio and generally lower elongation values. A low charcoal concentration (trough) is associated with increasing percentages of forest and heathland and temperature rise (Fig. 7).

To quantify the interpretation of association between pollen data and mean elongation curve, the same statistics were conducted (the effect of climate on elongation), revealing no significant differences between climate groups ($F = 0.886$, $p = 0.416$). The mean elongation values were 1.92 for heathland, 1.77 for Mediterranean forest, and 1.85 for semi-desert. Post-hoc Tukey tests confirmed no significant pairwise differences between the groups. A Welch test, accounting for unequal variances, also showed no significant effect of climate on elongation ($F = 0.545$, $p = 0.587$) (see Annex 1.1).

Peaks are graphically and statistically associated with semi-desert and Mediterranean forest. Further graphical interpretation shows increased fire activity with occurrence of IRD peaks (high Zr/Sr ratio) and generally lower elongation values, whereas the particle classification shows ligneous origin as the dominant fuel type.

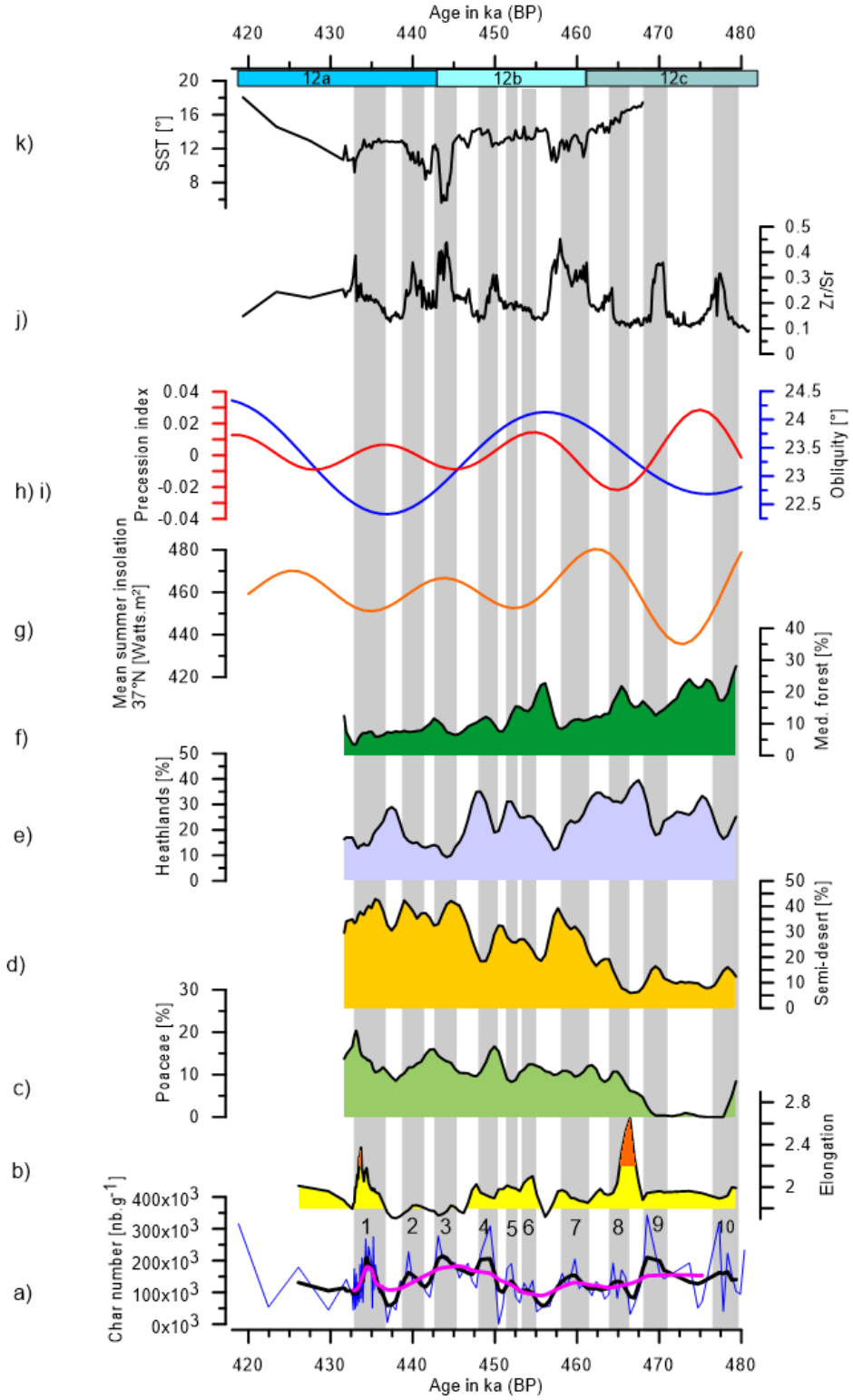

Figure 7 Microcharcoal concentration of core IODP U1385 (this study) compared with vegetation and with orbital parameters (418ka-480ka (BP)). a) Microcharcoal concentration of core IODP U1385 (this study) with a weighted curve (black line)with a window of 5 and a weighted curve (pink line) with a window of 15. b) Mean elongation curve of the microcharcoal particles averaged with a window of 5. Orange colour indicates values above 2.2 following the median value of Haliuc et al. (2023) to identify charcoal produced by open-grassland savanna fires versus dwarf open shrubland with scattered trees fires. This threshold is similar to the one used by Leys et al. (2015) and Aleman et al. (2013) (width/length of 0.5 corresponding to a length/width of 2). Yellow colour indicates values above 1.8 determined for distinction between grassland and shrub-tree vegetation (Genet, Daniau, personal communication). c) – f) vegetation proxies retrieved from pollen analyses (Naughton F., unpublished). g) mean summer insolation at 37°N (Berger, 1978). h) and i) Precession and obliquity (Berger, 1978). j) Zr/Sr ratio as IRD proxy from the same core (Hodell et al., 2023). k) Reconstructed SST of core IODP U1385 (Naughton, pers. communication). a)-f) a weighted average with a window of 5 was applied.

3.3 Comparison between charcoal, vegetation, orbital parameters and IRD deposits for MIS16

General trends for MIS 16 (Fig. 8) show that the Mediterranean forest decreases in percentage with temperature but has a slight increase getting closer to termination V with an exceptional peak at 645 ka. Heathland shows two large maxima at 637 ka and 660 ka. Semi-desert stays relatively constant over the time of the glacial with a trough at 635 ka. The curve of Poaceae describes a zig-zag pattern with stable percentages over time. There are six peaks in the Zr/Sr ratio at 625, 640, 662, 668, 671 and 679 ka respectively. SSTs show less fluctuation in comparison with MIS 12 and average at 13°C during the glacial. The averaged charcoal concentration stays relatively constant (cf. pink line Fig. 8), with a noticeable general long-term trend opposed to the curve of Mediterranean forest. Highest charcoal concentrations were found during peaks and increases of precession, e.g. peak 1 at 635 ka relates to a precessional index of 0.02 and peak 2 at 658ka corresponds to a precessional index of 0.03. The elongation curve shows three major peaks at 635, 648 and 652 ka, yet there seems to be no apparent connection to the vegetation taxa. There is no clear association visible between the mean elongation curve and the pollen data, however the coloured thresholds show some relation between the elongation degree and heathland as e.g. charcoal peaks 1 and 5, that are associated with peaks in heathland also relate to peaks in elongation.

Analysing Figure 8, charcoal concentration is peaking with heathland in 4/5 peaks. Furthermore, charcoal concentration peaks occur together with semi-desert peaks in 2/5 peaks, with Poaceae in 1/5 peaks and with Mediterranean forest in 3/5 peaks. Yet, the analysis of charcoal concentration across different climate conditions using ANOVA (see Annex 1.2) yielded an F-value of 0.449 and a p-value of 0.64, indicating that the mean charcoal concentration does not vary significantly by vegetation type. Descriptive statistics show that the mean charcoal concentration values are fairly consistent across the groups: heathland (109,301.3 nb.g^{-1}), Mediterranean forest (122,050.3 nb.g^{-1}), and semi-desert (100, 444.2 nb.g^{-1}), with standard deviations ranging from 69,079.82 to 90,841.03. Poaceae was not included due to its non-dominating character. Tukey's HSD test, which compares all pairs of climate conditions, also confirmed that there are no significant differences between groups, with all pairwise comparisons resulting in high p-values and confidence intervals that include zero. The Welch test (F-value of 0.425 and a p-value of 0.658), supports the conclusion that climate does not significantly affect charcoal concentration in this dataset (see Annex 1.2).

Graphical association however shows an overall pattern of individual charcoal peaks with, heathland, temperature, and Mediterranean forest (individual peaks, not overall curve) as well as with troughs in semi-desert. However, due to the large amplitude in oscillations, the significant peaks are difficult to distinguish, thus it was chosen to opt for the peaks that consist of several peaks, which makes precise association difficult.

A Pearson correlation test (see Annex 1.3) was performed to assess the relationship between charcoal concentration and elongation. The correlation coefficient was found to be -0.2499, indicating a weak negative relationship between the two variables. The result was statistically significant, with a t-value of -2.365 and a p-value of < 0.001, suggesting that the correlation is unlikely to be due to random chance. The 95 % confidence interval for the correlation ranged from -0.4385 to -0.0401, further confirming the presence of a negative association. This suggests that as charcoal concentration increases, elongation tends to decrease slightly, although the relationship is not strong. Additionally, the statistical analysis (ANOVA, Tukey, Welch, see Annex 1.2) was repeated for elongation and vegetation.

The ANOVA analysis (see Annex 1.2) on elongation across different climates indicates that while there are some differences in means, these differences are not statistically significant at the 5% level ($p = 0.0637$). The F-value of 2.846 suggests that vegetation might influence elongation to some extent albeit the association is not statistically significant. The descriptive statistics reveal that values of the mean elongation ratio are highest in heathland vegetation (mean of 2.12 (SD = 0.34, n = 20)), followed by semi-desert vegetation (mean elongation of 1.97 (SD = 0.36, n = 53)) and Mediterranean forest vegetation (mean elongation at 1.79 (SD = 0.51, n = 13)). While no overall significant differences between vegetation were detected in the ANOVA, Tukey's test indicated a marginally significant difference between Mediterranean forest and heathland ($p = 0.050$). Specifically, the estimated difference in elongation between Mediterranean and Heath was -0.322**,** with a confidence interval ranging from -0.644 to **-** 0.0001, suggesting a tendency for lower elongation in Mediterranean forest vegetation. However, no significant differences were observed between semi-desert and the other vegetation taxa.

Therefore, even though there is no statistically significant association between peaks, the graphical interpretation shows increased fire activity with heathland vegetation (wetter and cooler climate) and higher temperatures (absence of IRD peaks), whereby the particle classification shows ligneous origin as the main fuel type.

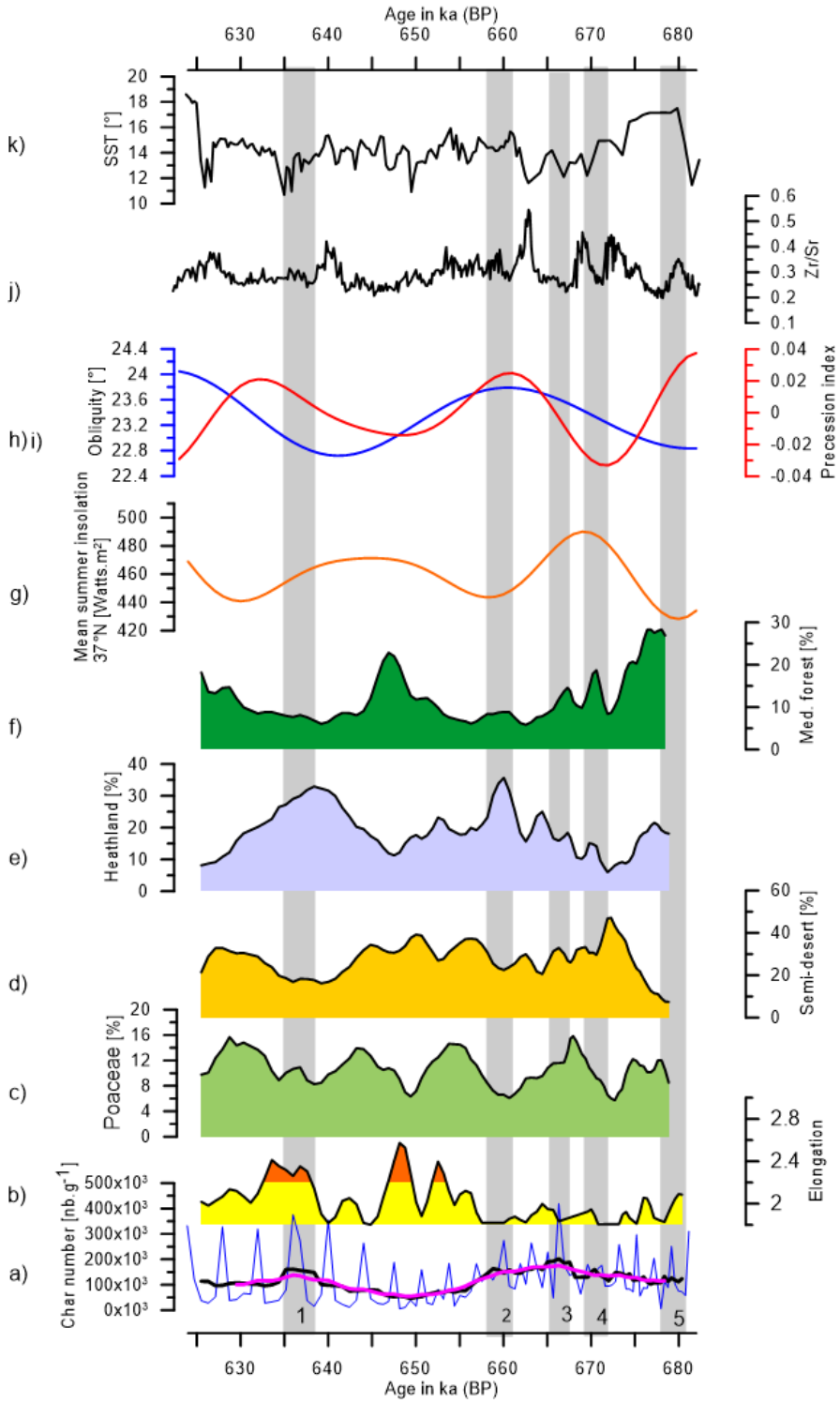

Figure 8 Microcharcoal concentration of core IODP U1385 (this study) compared with vegetation and with orbital parameters (624ka-683ka (BP)). a) Microcharcoal concentration of core IODP U1385 (this study)with a weighted curve (black line)with a window of 5 and a weighted curve (pink line) with a window of 15. b) Mean elongation curve of the microcharcoal particles averaged with a window of 5. Orange colour indicates values above 2.2 following the median value of Haliuc et al. (2023) to identify charcoal produced by open-grassland savanna fires versus dwarf open shrubland with scattered trees fires. This threshold is similar to the one used by Leys et al. (2015a) and Aleman et al. (2013) (width/length of 0.5 corresponding to a length/width of 2). Yellow colour indicates values above 1.8 determined for distinction between grassland and shrub-tree vegetation (Genet, Daniau, personal communication). c) – f) vegetation proxies retrieved from pollen analyses (Naughton, unpublished). g) mean summer insolation at 37°N (Berger, 1978). h) and i) Precession and obliquity (Berger, 1978). j) Zr/Sr ratio as IRD proxy from the same core (Hodell et al., 2023). k) Reconstucted SST of core IODP U1385 (Naughton, pers. communication). a)-f) a weighted average with a window of 5 was applied.

4. Discussion

The charcoal concentration and morphology analysed previously provide information about fire intensity, frequency and also about the types of vegetation that were more susceptible to burning during specific climatic conditions. The presence of peaks in the charcoal record also reflects the intermittent nature of fire events, likely influenced by both internal (vegetation composition) and external (climatic) drivers.

To identify the origin of charcoal particles, two thresholds were applied in this study, above 2.2 indicating fires in Africa predominantly fuelled by grasses (Haliuc *et al.* (2023), and a threshold of 1.8 which indicates the same origin, however more focused on vegetation in the Mediterranean region (Genet & Daniau, unpub.). Additionally, particle classification following Vachula *et al.* (2021) was applied. During MIS 12, two elongation peaks were above 2.2, and the other peaks surpassed the value of 1.8 thus showing characteristics for the burning of grassland environments. In MIS 16, the elongation values show more peaks surpassing both thresholds suggesting more presence of grass fires, yet not necessarily related to charcoal peaks. The use of these thresholds offers valuable insights into fire dynamics, but it is important to acknowledge their limitations. Fires in woody environments, while still contributing charcoal to the record, tend to produce smaller, more fragmented particles. The transportation of charcoal particles can influence their morphology, particularly in terms of elongation and size. Charcoal from more distant fires can fragment during transport, which may reduce the apparent elongation values (Frank-DePue *et al.*, 2023). However, in this study, the strong correlation between charcoal concentration and surface area ($r = 0.964$ for MIS 16, $P<0.001$) and $r= 0.897$ for MIS 12, $P<0.001$, see Fig. 5) suggests that fragmentation due to long-distance transport did not significantly bias the data. This supports the interpretation that much of the charcoal originated from regional fires, minimizing the impact of transportation on the overall morphological signature. The threshold established by Genet & Daniau was established for Mediterranean ecosystems, thus should be more fitting for this study. However following this threshold there is little to no difference in origin of the particles, whereas the classification from Haliuc *et al.* (2023) would show more varied origins. The Vachula (2021) particle classification enables more exhaustive interpretations. It shows that most particles were produced by ligneous vegetation but it also confirms that peaks in elongation (or more elongated values) indicate the burning of graminoid/shrubs during certain periods.

In MIS 12 (cf. Fig 7), peaks in microcharcoal concentration are generally associated with semi-desert vegetation and increasing forest cover. Notably, peaks in the Zr/Sr ratio, indicating ice-rafted debris (IRD) events, often coincide with microcharcoal peaks, suggesting that cold events were linked to increased wildfire activity. Moments of increased fire activity correspond to the peaks in semi-desert vegetation, which can be seen as an indicator of dry climates. Semi-desert vegetation is next to heathlands the most abundant in terms of pollen percentages, yet the particle classification has shown that ligneous fuel makes up most of the burnt particles and hence seems to burn better. Thus, ligneous fuel was increasingly burning under dry conditions during MIS 12, likely driven by cool, dry glacial conditions that promoted such vegetation.

When regarding the same curves for MIS 16, (cf. Fig 8) there is a stronger association of charcoal concentration to heathland, albeit the percentage in pollen is higher for semi-desert vegetation during the glacial. So, even though the climate was on average more dominated by semi-desert vegetation, fire activity increased when climate conditions were more favourable for heathland. The particle classification characteristics are comparable to the one of MIS 12 regarding the behaviour of ligneous fuel. Therefore, albeit the average elongation curve shows mainly grassland-produced fuel (following the thresholds of Genet & Daniau) it is again ligneous fuel (Vachula classification) that is burning in majority under climatic conditions favourable for heathland vegetation.

Presently, fire activity intensifies during severe summer droughts associated with persistent anticyclonic conditions. Traditional interpretations for the Holocene imply that periods of heightened fire regime signify severe drought episodes (Turco et al., 2019; Ruffault, 2020). In southwestern Iberia, throughout the Last Glacial Period (70-14 ka), wetter and warmer interstadials are characterised by increased fire activity associated with open Mediterranean forest, while drier stadials and Heinrich Events (HEs) are associated with diminished fire activity associated with semi-desert vegetation (Daniau *et al.*, 2007). This finding seem to also fit MIS 16, however MIS 12 exhibits the opposite pattern of higher fire activity during IRD events (more arid conditions), yet the fuel availability is associated with ligneous fuel and Mediterranean forest vegetation. Thus, it is likely that Mediterranean forest made up the general fuel and the occurrence/dominance of semi-desert vegetation indicated periods of aridification that promoted ignition. These differences in fire regime behaviour indicate that there must be differences in response mechanisms such as the different internal and/or external forcing factors such as atmospheric circulations and orbital variability (and MIS 16 being potentially more similar to the Last Glacial Period).

External forcing factors such as the precession and obliquity cycles exhibit distinct patterns, with higher amplitudes of solar radiation and precession index during MIS 16 but less precession minima than MIS 12, while obliquity shows higher amplitude during MIS 12. High obliquity corresponds to high seasonal contrast whereas low obliquity signifies less seasonality and thus milder seasons. Precession on the other hand modulates seasonality as well, albeit in a counter-hemispheric matter, i.e. a low precession index implies more extreme seasons in the northern hemisphere and less extreme seasons in the southern hemisphere and vice versa for a high precession index (Ruddiman, 2001). A reduced seasonality potentially reduces fire activity because summers would be more humid and less conducive to the large-scale burning of vegetation. Minimum precession increases seasonality in the northern hemisphere, hence promotes the growth of vegetation during wetter winters (Tuenter *et al.*, 2005) which becomes fuel for fires during subsequent drier summers. During MIS 16, precession maxima aligned with heathland vegetation peaks, which was graphically associated to long periods of increased fire activity (pink curve in Fig. 8). Here, it seems that the reduced seasonality supports the opening of the Mediterranean forest and the development of heathland, i.e. open Mediterranean woodlands, a vegetation which burns easily that might favour fire activity. Whereas during precession minima, an increase in seasonality might favour the development of a closed Mediterranean forest that limits the spread of fires and might explain less fire activity at 680-675, 655-645 and 630 ka. During MIS 12 however, there is no apparent connection in pollen percentages and precession or charcoal concentration and precession, thus making it more difficult to interpret. This could be related to the fact that the amplitude of precession is smaller during MIS 12 than during MIS 16. However, Rodrigues *et al.*, (2017) stated that the high precession forcing during MIS 12 (more minima than during MIS 16) is likely to have led to an enhanced fresh water input from the melting of the European ice sheets via the Portugal current at site U1385. This in turn influenced the occurrence of cold events which is reflected in the higher frequency and amplitude of peaks of the Zr/Sr ratio indicating the IRD events (cf. Figure 6).

Glacial fire activity over the entire MIS 12 and 16 likely reflect the combined effects of vegetation type, as well as climatic shifts driven by AMOC shut-down and a AF positioning. One of the internal forcing factors, the AMOC, which governs heat and moisture distribution in the North Atlantic, is likely to have influenced fire regimes during the studied periods. A weakened AMOC, typically associated with glacial periods, would lead to cooler, drier conditions in southern Europe (Bellomo *et al.*, 2023), promoting the spread of fire-prone

vegetation such as grasses and shrubs which is particularly evident during MIS 12. During MIS 16, the North Atlantic Overturning Circulation however was likely greater compared to MIS 12, possibly due to the relatively high SSTs (Naafs, 2011; cf. Fig. 8 curve k) and confirmed by a northwest position of the AF compared to a southward position during MIS 12 (Rodrigues *et al.*, 2017). The influence of wetter climatic conditions during MIS 16 thus may have promoted more woody and shrub vegetation (open Mediterranean woodland and closed Mediterranean forest), which burns less readily than grasses and resulted in less fire activity. Intensified summer heat due to precession minima may exacerbated drought conditions, drying out vegetation and increasing the likelihood of wildfires. Thus, during MIS 12, a higher number of precession minima might have contributed globally to hotter summers, reducing moisture availability and promoting the spread of fire-prone vegetation. The Mediterranean forests shrank, and more drought-resistant vegetation such as grasses and shrubs dominated, leading to increased wildfire activity.

MIS16 on the other hand is more similar to the Last Glacial Period concerning the strength of AMOC (Böhm *et al.*, 2015). For both glacial periods the AMOC stayed considerably strong meaning that the climate was warmer and wetter than when compared to glacial periods with AMOC shutdown that caused the AF to shift southwards as in MIS 12 (climate colder and drier). The dominance of heathland and Mediterranean forest attests of a warmer and wetter climate (Naughton, unpub.). Within MIS 16 fire activity increased during periods of increased heathland vegetation. Thus, the behaviour of the charcoal – heathland interaction is more connected to the apparent paradox of increased fire activity during wetter instead of drier periods as described by Daniau *et al.* (2007) for the Last Glacial Period.

An additional internal forcing factor of climate is atmospheric circulation such as the North Atlantic Oscillation (NAO) that profoundly influences wintertime temperature and precipitation patterns across the North Atlantic. In its positive phase, the Mediterranean region experiences significant drought due to the northward shift of westerly winds, while a negative phase brings increased humidity as weaker westerlies move southward (Mariotti & Arkin, 2007). Previous research has suggested a prevailing positive NAO-like situation during stadials and HEs in the Iberian Peninsula resulting in arid conditions and a low fire activity due to the burning of semi-desert vegetation (Daniau *et al.*, 2007). Whereas, during interstadials, fires are hypothesized to spread in Mediterranean forest and heathland under a negative NAO (Daniau *et al.*, 2007). As MIS 12 showed particularly cold temperatures as modulated by AMOC breakdown and AF position shift (south), the findings for stadial events of the Last Glacial Period can potentially

be extrapolated to the behaviour of the charcoal-vegetation relation during the glacial MIS 12, i.e. burning during arid conditions potentially linked to a positive NAO-like pattern. Yet, during MIS 12, fires did not propagate through semi-desert vegetation but through ligneous vegetation under an arid climate and showed increased fire activity during stadial events instead of interstadials. This difference between MIS 12 and the Last Glacial Period could be attributed to different climatic conditions, such as a potentially drier climate during the Last Glacial Period. When regarding mean values of pollen for Mediterranean forest, semi-desert vegetation and heathland vegetation, the Last Glacial period shows the highest values of semi-desert vegetation, and lowest values of Mediterranean forest (see Fig.9) (Pair-wise T-test for the mean; p-value<0.05, see Annex 2.), which indicates a drier regional climate.

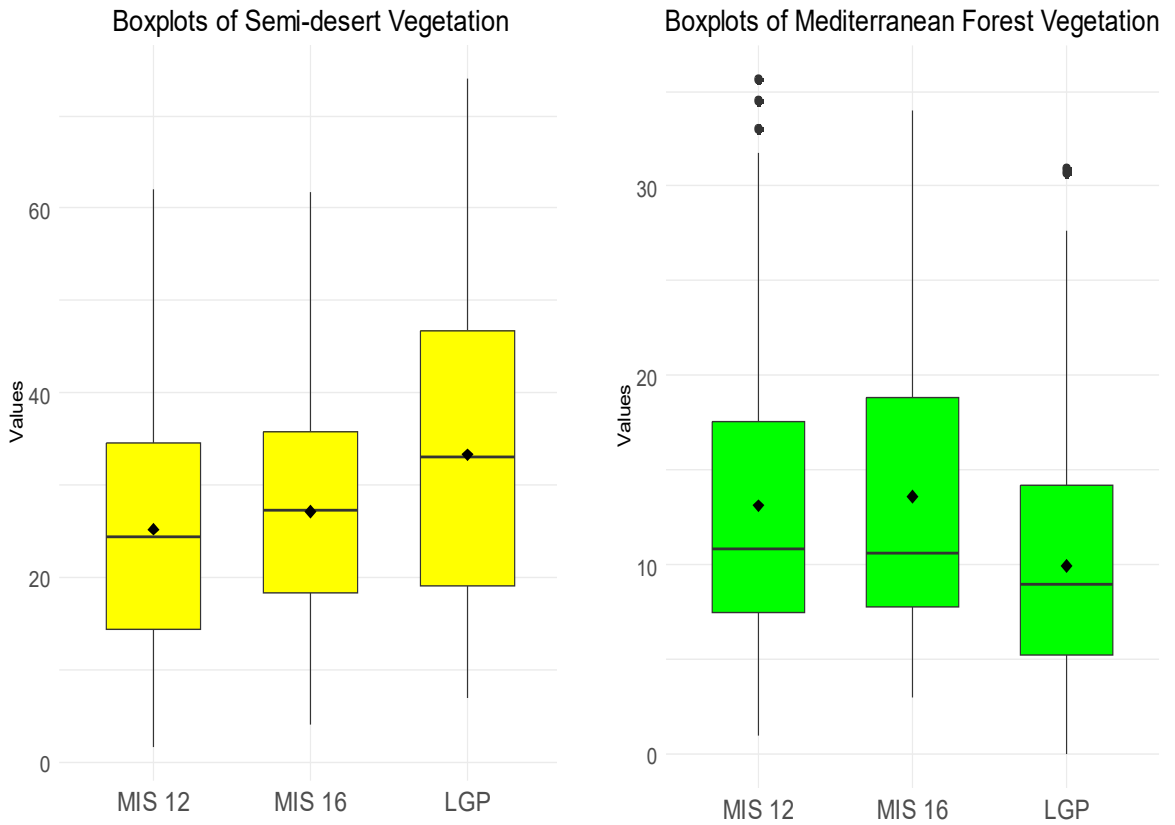

Figure 9 Boxplots of pollen concentration for semi-desert and Mediterranean forest for MIS 12, MIS 16 (Naughton, unpub.) and the Last Glacial Period (Sánchez Goñi et al. (2000) and Sánchez Goñi (2006) except for the interval 14,000 and 25,000 yr where theycome from the twin core SU81-18 (Lezine and Denefle, 1997).).Left: Semi-desert vegetation. Right: Mediterranean forest vegetation

The higher fire activity during IRD events in MIS 12 under drier conditions, compared to the wetter, heathland-dominated fire regimes in MIS 16, shows how differently these stages responded to climatic shifts. Hence, different fire regimes/responses can be identified. For instance, the fire activity during MIS 12 could be characterised as a fuel-moisture limited

system as described by Karp *et al.* (2023), meaning that fire activity increased during dry periods increasing the flammability of the Mediterranean forest vegetation. Following Karp *et al.* (2023) classification, MIS 16 could be characterised as a fuel-load limited system, as fire activity increased during wetter and warmer periods. However, it seems that fire activity is more driven by the development of open Mediterranean woodlands, suggesting that fire is steered by the shift in vegetation types (closed Mediterranean forest versus open Mediterranean woodlands). This pattern resembles also the "fuel-moisture limited to fire excluded" system described by Karp *et al.* (2023). When the fuel is too wet (closed Mediterranean forest), fire is excluded whereas decreasing rainfall (open Mediterranean woodlands) increases fire.

This classification following Karp *et al.* (2023) can also help to understand the differences between MIS 12 and the Last Glacial Period with regards to fire activity during positive NAO-like conditions during stadials (cf. above). With the Last Glacial period potentially being drier than MIS 12 it could be concluded that the fire activity was more fuel-load limited when compared to the fuel-moisture limited activity of MIS 12.

These differences in fire activity could indicate more importance of obliquity and precession forced mechanisms related to atmospheric circulations and AMOC position when it comes to the modulation of climatic shifts than previously assumed. As such, a higher precession index during MIS 16 could have led to a climatic shift in atmospheric circulation that caused the AF to shift northwest instead of south and thus making SW Iberia wetter and less fire-prone when compared to MIS 12 (making the fire regime fuel-moisture limited to fire excluded). Whereas during MIS 12 the AF shifted southwards causing aridification and therefore causing the fire activity to shift totally towards a fuel-moisture limited regime.

5. Conclusion

This research aimed to deepen the understanding of past climate dynamics, focusing on MIS 12 and MIS 16, with a primary objective of documenting changes in biomass burning and wildfire regimes during these periods. Through microcharcoal analysis, the study examined fluctuations in fire activity and their relationship with vegetation type and climate conditions. The integration of data from the Hydroshifts project provided comprehensive insights into the coupled atmosphere-ocean-terrestrial interactions at IODP Site U1385. By conducting morphological analyses of charcoal particles, patterns of fire activity and the vegetation types most susceptible to burning during these glacial periods were identified.

The elongation thresholds of 2.2 and 1.8, used to distinguish grassland fires, indicated that grass-dominated vegetation likely contributed significantly to fire activity, particularly during MIS 12. This period was characterised by association of increases in charcoal activity with increases in semi-desert vegetation indicating a dry climate. This climate was driven by a weakened Atlantic Meridional Overturning Circulation (AMOC) and the southward shift of the Arctic Front, leading to aridification in SW Iberia. A higher number of precession minima might have contributed globally to hotter summers, reducing moisture availability and promoting the spread of fire-prone vegetation. Statistical analysis and graphical inspection showed an association between increased fire activity and peaks in semi-desert vegetation during dry periods.

In contrast, MIS 16 displayed less fire activity, with elongation values suggesting both grass and woody vegetation burning but with greater climatic stability, reducing overall fire intensity. MIS 16 was influenced by higher amplitude of precession values and a relatively stable AMOC, leading to wetter conditions that promoted fire-resistant woody vegetation. Although peaks in heathland were associated with increased fire activity, no statistical significance was found.

Following the classification by Karp et al. (2023), MIS 12 could be characterised as a fuel-moisture limited system as fire activity increased during dry periods which enhanced the flammability of the Mediterranean forest vegetation. The fire activity during MIS 16 is likely driven by the shift in vegetation types (closed Mediterranean forest versus open Mediterranean woodlands) which can be characterised as “fuel-moisture limited to fire excluded” system described by Karp *et al.* (2023).

The comparison between MIS 12 and the Last Glacial Period (LGP) suggests that the LGP, being drier, may have been more fuel-load limited than the fuel-moisture limited conditions of MIS 12. These differences highlight the potential importance of obliquity and precession-forced mechanisms, particularly on atmospheric circulations and AMOC position, in modulating climatic shifts. A higher amplitude of the precession index during MIS 16 may have caused a shift in atmospheric circulation that led to a northwestward shift in the Arctic Front, making SW Iberia wetter and less fire-prone compared to the southward shift during MIS 12, which led to aridification and a fuel-moisture limited fire regime.

Overall, this study underscores the complex interactions between vegetation, fire regimes, and climate during glacial periods and how these are modulated by internal, as well as external forcing factors. Future research opportunities lie especially in higher resolution analyses of glacial terminations V and VII to gain further knowledge of fire regimes and their responses to non-linear behaviour of the climate system.

References

ACER project members; Sanchez Goñi, M. F., Desprat, S., Daniau, A-L., Eynaud, F., Turon, J-L., Shackleton, N., Landais, A., Cacho, I., Duprat, J.M., Rossignol, L. & Gendreau, S (2017). CLAM age model and pollen profile of sediment core MD95-2042 [dataset]. PANGAEA, https://doi.org/10.1594/PANGAEA.872899

Aleman, J. C., Blarquez, O., Bentaleb, I., Bonté, P., Brossier, B., Carcaillet, C., ... & Favier, C. (2013). Tracking land-cover changes with sedimentary charcoal in the Afrotropics. *The Holocene*, *23*(12), 1853-1862.

Alonso García, M. (2010). Cambios climáticos a escala orbital y milenaria en el Atlántico norte entre 800.000 y 400.000 años. Universidad de Salamanca.

Alonso Garcia, M., Sierro, F.J., Flores, J.A., 2011. Arctic front shifts in the subpolar North Atlantic during the Mid-Pleistocene (800-400 ka) and their implications for ocean circulation. Palaeogeogr. Palaeoclimatol. Palaeoecol. 311, 268-280,

Alonso Garcia, M., Sierro, F. J., Kucera, M., Flores, J. A., Cacho, I., & Andersen, N. (2011a). Ocean circulation, ice sheet growth and interhemispheric coupling of millennial climate variability during the mid-Pleistocene (ca 800–400 ka). *Quaternary Science Reviews*, *30*(23-24), 3234-3247.

Arneth, A., Harrison, S. P., Zaehle, S., Tsigaridis, K., Menon, S., Bartlein, P. J., ... & Vesala, T. (2010). Terrestrial biogeochemical feedbacks in the climate system. *Nature Geoscience*, *3*(8), 525-532. Arneth, A., Harrison, S. P., Zaehle, S., Tsigaridis, K., Menon, S., Bartlein, P. J., ... & Vesala, T. (2010). Terrestrial biogeochemical feedbacks in the climate system. *Nature Geoscience*, *3*(8), 525-532.

Beaufort, L., de Garidel-Thoron, T., Linsley, B., Oppo, D., Buchet, N., 2003. Biomass burning and oceanic primary production estimates in the Sulu Sea area over the last 380 kyr and the East Asian Monsoon Dynamics. Marine Geology 201, 53–65

Bellomo, K., Meccia, V.L., D'Agostino, R. *et al.* (2023). Impacts of a weakened AMOC on precipitation over the Euro-Atlantic region in the EC-Earth3 climate model. *Clim Dyn* **61**, 3397–3416. https://doi.org/10.1007/s00382-023-06754-2

Berger, A. (1978). Long-term variations of daily insolation and Quaternary climatic changes. *Journal of Atmospheric Sciences*, *35*(12), 2362-2367.

Billups, K. and A. Scheinwald, 2014, Origin of millennial-scale climate signals in the subtropical North Atlantic, Paleoceanography, 29, 612–627, DOI:10.1002/2014PA002641.

Bird, M.I., Cali, J.A., 1998. A million-year record of fire in sub-Saharan Africa. Nature 394, 767–769.

Black, M.P., Mooney, S.D., Martin, H.A., (2006). A 443,000-year vegetation and fire history from Lake Baraba, New South Wales, Australia. Quaternary Science Reviews 25, 3003–3016.

Blackford, J. J. (2000). Charcoal fragments in surface samples following a fire and the implications for interpretation of subfossil charcoal data. *Palaeogeography, palaeoclimatology, palaeoecology*, *164*(1-4), 33-42.

Böhm, E., Lippold, J., Gutjahr, M., Frank, M., Blaser, P., Antz, B., ... & Deininger, M. (2015). Strong and deep Atlantic meridional overturning circulation during the last glacial cycle. *Nature*, *517*(7532), 73-76.

Bosmans, J. H. C., Drijfhout, S. S., Tuenter, E., Lourens, L. J., Hilgen, F. J., & Weber, S. L. (2012). Monsoonal response to mid-holocene orbital forcing in a high resolution GCM. *Climate of the Past*, *8*(2), 723-740.Brauer, A., Haug, G.H., Dulski, P., Sigman, D.M. and Negendank, J.F.W., 2008. An abrupt wind shift in Western Europe at the onset of the Younger Dryas cold period. Nature Geoscience 1, 520-523. DOI: 10.1038/ngeo263

Bowman, D. M., Balch, J. K., Artaxo, P., Bond, W. J., Carlson, J. M., Cochrane, M. A., ... & Pyne, S. J. (2009). Fire in the Earth system. *science*, *324*(5926), 481-484.

Caesar, L., Rahmstorf, S., Robinson, A., Feulner, G., Saba, V., 2018. Observed fingerprint of a weakening Atlantic ocean overturning circulation. Nature 556 (7700), 191. https://www.nature.com/articles/s41586-018-0006-5.

Carmona-Moreno, C., Belward, A., Malingreau, J.-P., Hartley, A., Garcia-Allegre, M., Antonovskiy, M., Buchshtaber, V., Pivovarov, V., 2005. Characterizing interranual variations in global fire calendar using data from Earth observing satellites. Global Change Biology 11, 1537–1555.

Cayre, O., Lancelot, Y., Vincent, E., Hall, M.A., 1999. Paleoceanographic reconstructions from planktonic foraminifera off the Iberian margin: temperature, salinity and Heinrich events. Palaeoceanography 14, 384–396.

Clark, J.S., Goldammer, J.G., Stocks, B., 1997. Sediment Records of Biomass Burning and Global Change. NATO ASI Series, Series No. 1(51). Springer, Berlin, 489pp

Conedera, M., Tinner, W., Neff, C., Meurer, M., Dickens, A. F., & Krebs, P. (2009). Reconstructing past fire regimes: methods, applications, and relevance to fire management and conservation. *Quaternary Science Reviews*, *28*(5-6), 555-576.

Crutzen, P.J., Heidt, L.E., Krasnec, J.P., Pollock, W.H., Seiler, W., 1979. Biomass burning as a source of atmospheric gases CO, H2, N2O, NO, CH3Cl and COS. Nature 282, 253–256.

Daniau, A.L., Sánchez Goñi, M.-F., Beaufort, L., Laggoun-Défarge, F., Loutre, M.-F., Duprat, J., 2007. Dansgaard-Oeschger climatic variability revealed by fire emissions in southwestern Iberia. Quaternary Science Reviews 26, 1369–1383.

Daniau A-L., Desprat S., Aleman J.C., Bremond L., Davis, B., Fletcher W., Marlon J.R., Marquer L., Montade V., Morales Del Molino, C., Naughton F., Rius D., Urrego D.H. 2019. Terrestrial plant microfossils in paleoenvironmental studies, pollen, microcharcoal and phytolith. Towards a comprehensive

understanding of vegetation, fire and climate changes over the past one million years. Revue de micropaléontologie, SCImago Journal Rank (SJR): 0.533. https://doi.org/10.1016/j.revmic.2019.02.001

Denton, G.H., Anderson, R.F., Toggweiler, J.R., Edwards, R.L., Schaefer, J.M., Putnam, E., 2010. The last glacial termination. Science 328, 1652–1656. DOI: 10.1126/science.1184119

Fletcher, W. J., & Sánchez Goñi, M. F. (2008). Orbital- and sub-orbital-scale climate impacts on vegetation of the western Mediterranean basin over the last 48,000 yr. *Quaternary Research*, *70*(3), 451–464. doi:10.1016/j.yqres.2008.07.002

Frank-DePue, L., Vachula, R. S., Balascio, N. L., Cahoon, K., & Kaste, J. M. (2023). Trends in sedimentary charcoal shapes correspond with broad-scale land-use changes: insights gained from a 300-year lake sediment record from eastern Virginia, USA. *Journal of Paleolimnology*, *69*(1), 21-36.

Ganopolski, A., Rahmstorf, S., 2001. Rapid changes of glacial climate simulated in a coupled climate model. Nature 409, 153–58. DOI:10.1038/35051500

Gendreau, S., 1999. Les de´ba^cles d'iceberg au large du Portugal sur le dernier cycle climatique: re´ponse du continent et des environnements oce´aniques. Master (DEA) Thesis, Universite´ Bordeaux1, Talence, France.

Giorgi, F., Lionello, P., 2008. Climate change projections for the Mediterranean region. Global and Planetary Change 63, 90-104. DOI: 10.1016/j.gloplacha.2007.09.005

Haliuc, A., Daniau, A. L., Mouillot, F., Chen, W., Leys, B., David, V., ... & Crosta, X. (2023). Microscopic charcoals in ocean sediments off Africa track past fire intensity from the continent. *Communications Earth & Environment*, *4*(1), 133.

Harrison, S., Goñi, M.S., 2010. Global patterns of vegetation response to millennial-scale variability and rapid climate change during the last glacial period. Quaternary Science Reviews 29, 2957–2980

Harrison, S. P., Prentice, I. C., & Bartlein, P. J. (1992). Influence of insolation and glaciation on atmospheric circulation in the North Atlantic sector: implications of general circulation model experiments for the Late Quaternary climatology of Europe. *Quaternary Science Reviews*, *11*(3), 283-299.

Head, M. J., & Gibbard, P. L. (2005). Early-Middle Pleistocene transitions: an overview and recommendation for the defining boundary. *Geological Society, London, Special Publications*, *247*(1), 1-18.

Hodell, D. A., Channell, J. E., Curtis, J. H., Romero, O. E., & Röhl, U. (2008). Onset of "Hudson Strait" Heinrich events in the eastern North Atlantic at the end of the middle Pleistocene transition (~ 640 ka)?. *Paleoceanography*, *23*(4).

Hodell, D., Lourens, L., Crowhurst, S., Konijnendijk, T., Tjallingii, R., Jiménez-Espejo, F., Skinner, L., Tzedakis, P.C., Abrantes, F., et al. (2015). A reference time scale for Site U1385 (Shackleton Site) on the SW Iberian Margin., 2015. Global and Planetary Change 133, 49-64. DOI:10.1016/j.gloplacha.2015.07.002

Hodell, D. A., Crowhurst, S. J., Lourens, L., Margari, V., Nicolson, J., Rolfe, J. E., ... & Wolff, E. W. (2023). A 1.5-million-year record of orbital and millennial climate variability in the North Atlantic. *Climate of the Past*, *19*(3), 607-636.

Hollaar, T.P., Baker, S.J., Hesselbo, S.P. *et al.* (2021). Wildfire activity enhanced during phases of maximum orbital eccentricity and precessional forcing in the Early Jurassic. *Commun Earth Environ* **2**, 247. https://doi.org/10.1038/s43247-021-00307-3

IPCC (2012) In: Field CB, Barros V, Stocker TF, Qin D, Dokken DJ, Ebi KL, Mastrandrea MD, Mach KJ, Plattner G-K, Allen SK, Tignor M, Midgley PM (eds) Managing the risks of extreme events and disasters to advance climate change adaptation. A special report of working groups I and II of the Intergovernmental Panel on Climate Change (IPCC). Cambridge University Press, Cambridge, UK/New York, p 582

JRC, 2014. Joint Research Centre (JRC) of Science for Disaster Risk Reduction of the European Commission's. Mortara, B., Gonzalez Verdesoto, E., Barry, G. 2014. Science for Disaster Risk Reduction. DOI: 10.2788/65084.

Karp, A. T., Uno, K. T., Berke, M. A., Russell, J. M., Scholz, C. A., Marlon, J. R., ... & Staver, A. C. (2023). Nonlinear rainfall effects on savanna fire activity across the African Humid Period. *Quaternary Science Reviews*, *304*, 107994.

Kershaw, P., van der Kaars, S., Moss, P., Wang, S., 2002. Quaternary records of vegetation, biomass burning, climate and possible human impact in the Indonesian–Northern Australian region. In: Kershaw, P., David, B., Tapper, N., Penny, D., Brown, J. (Eds.), Bridging Wallace's Lines: The Environmental and Cultural History and Dynamics of the SE-Asian–Australian Region. Advances in Geoecology, Vol. 34. Catena Verlag, Reiskirchen, Germany, pp. 97–118.

Koutsodendris, A., Kousis, I., Peyron, O., Wagner, B., & Pross, J. (2019). The Marine Isotope Stage 12 pollen record from Lake Ohrid (SE Europe): Investigating short-term climate change under extreme glacial conditions. *Quaternary Science Reviews*, *221*, 105873.

Leys, B., Brewer, S. C., McConaghy, S., Mueller, J., & McLauchlan, K. K. (2015). Fire history reconstruction in grassland ecosystems: amount of charcoal reflects local area burned. *Environmental Research Letters*, *10*(11), 114009.

Lézine, A.-M., Denèfle, M., 1997. Enhanced anticyclonic circulation in the eastern North Atlantic during cold intervals of the last deglaciation inferred from deep-sea pollen records. Geology 25, 119–122.

Lionello, P. (Ed.). (2012). *The climate of the Mediterranean region: From the past to the future*. Elsevier.

Lobert, J.M., Scharffe, D.H., Hao, W.M., Crutzen, P.J., 1990. Importance of biomass burning in the atmospheric budgets of nitrogen-containing gases. Nature 346, 552–554.

Loidi, J. (Ed.). (2017). *The vegetation of the Iberian Peninsula* (Vol. 1). Cham: Springer.

Mariotti, A., Arkin, P. (2007). The North Atlantic Oscillation and oceanic precipitation variability. *Clim Dyn* **28**, 35–51. https://doi.org/10.1007/s00382-006-0170-4

Masson-Delmotte, V., M. Schulz, A. Abe-Ouchi, J. Beer, A. Ganopolski, J.F. González Rouco, et al., 2013: Information from Paleoclimate Archives. In: Climate Change 2013: The Physical Science Basis. Contribution of Working Group I to the Fifth Assessment Report of the Intergovernmental Panel on Climate Change [Stocker, T.F., et al and P.M. Midgley (eds.)]. Cambridge University Press, Cambridge, United Kingdom and New York, NY, USA.

Naafs, B. D. A., Stein, R., Hefter, J., Khélifi, N., De Schepper, S., & Haug, G. H. (2010). Late Pliocene changes in the North Atlantic current. *Earth and Planetary Science Letters*, *298*(3-4), 434-442

Naafs, B. D. A., Hefter, J., Ferretti, P., Stein, R., & Haug, G. H. (2011). Sea surface temperatures did not control the first occurrence of Hudson Strait Heinrich Events during MIS 16. *Paleoceanography*, *26*(4).

Naafs, B. D. A., Hefter, J., & Stein, R. (2013a). Millennial-scale ice rafting events and Hudson Strait Heinrich (-like) Events during the late Pliocene and Pleistocene: a review. *Quaternary Science Reviews*, *80*, 1-28..

Naafs, B. D. A., Hefter, J., Gruetzner, J., & Stein, R. (2013b). Warming of surface waters in the mid-latitude North Atlantic during Heinrich events. *Paleoceanography*, *28*(1), 153-163.

Naughton F., Sánchez Goñi, M.F., Kageyama, M., Bard, E., Cortijo, E., Desprat, S. , Duprat, J., Malaizé, B., Joli, C., Rostek, F. and Turon, J-L. , 2009. Wet to dry climatic trend in north western Iberia within Heinrich events. Earth and Planetary Science Letters. 284, 329-342. DOI:10.1016/j.epsl.2009.05.001

Naughton, F., Sanchez Goñi, M.F., Rodrigues, T., Salgueiro, E., Costas, S., Desprat, S., Duprat, J., Michel, E., Rossignol, L., Zaragosi, S., Abrantes, F., 2016. Climate variability across the last deglaciation in NW Iberia and its margin. Quaternary International 414, 9-22, DOI: 10.1016/j.quaint.2015.08.073

Naughton F., Costas S., Gomes S.D., Rodrigues T., Desprat S.., Bronk-Ramsey C., Salgueiro E., Sanchez Goñi M.F., Renssen H., Trigo, R., Oliveira, D., Voelker A.H.L., Abrantes F. 2019. Coupled ocean and atmospheric changes during the Younger Dryas in southwestern Europe. Quaternary science Reviews 212, 108-120. https://doi.org/10.1016/j.quascirev.2019.03.033.

Ng, H.C., Robinson, L.F., McManus, J.F., Mohamed, K.J., Jacobel, A.W., Ivanovic, R.F., Gregoire, L.J., Chen, T., 2018. Coherent deglacial changes in western Atlantic Ocean circulation. Nat. Commun. 9 (1). https://doi.org/10.1038/s41467-018-05312

Pages 2016. Interglacials of the last 800,000 years. Reviews of Geophysics https://doi.org/10.1002/2015RG000482

Pereira, M.G., Trigo, R.M., da Camara, C.C., Pereira, J.M.C., Leite, S.M., 2005. Synoptic patterns associated with large summer forest fires in Portugal. Agricultural and Forest Meteorology 129, 11–25.

R Core Team (2023). _R: A Language and Environment for Statistical Computing_. R Foundation for Statistical Computing, Vienna, Austria. <https://www.R-project.org/>.

Renssen, H., and Isarin, R.F.B., 1997. Surface temperature in NW Europe during the Younger Dryas: AGCM simulation compared with temperature reconstruction. Climate Dynamics 14, 33-44. DOI: 10.1007/s003820050206

Renssen, H., Mairesse, A., Goosse, H., Mathiot, P., Heiri, O., Roche, D.M., Nisancioglu, K.H., Valdes, P.J., 2015. Multiple causes of the Younger Dryas cold period. Nature Geosciences 8, 946-949. https://doi.org/10.1038/ngeo2557

Rodrigues, T., Alonso-García, M., Hodell, D. A., Rufino, M., Naughton, F., Grimalt, J. O., ... & Abrantes, F. (2017). A 1-Ma record of sea surface temperature and extreme cooling events in the North Atlantic: A perspective from the Iberian Margin. *Quaternary Science Reviews*, *172*, 118-130.

Ruddiman, W. F. (2001). *Earth's Climate: past and future*. Macmillan.

Ruffault, J., Curt, T., Moron, V., Trigo, R. M., Mouillot, F., Koutsias, N., ... & Belhadj-Khedher, C. (2020). Increased likelihood of heat-induced large wildfires in the Mediterranean Basin. *Scientific reports*, *10*(1), 13790.

Sánchez Goñi, M.F., Cacho, I., Turon, J.-L., Guiot, J., Sierro, F.J., Peypouquet, J.-P., Grimalt, J.O., Shackleton, N.J., 2002. Synchroneity between marine and terrestrial responses to millennial scale climatic variability during the Last Glacial Period in the Mediterranean region. Climate Dynamics 19, 95–105.

Sanchez Goni, M.F., Eynaud, F., Turon, J.-L., Shackleton, N.J., 1999. High resolution palynological record off the Iberian margin: direct land-sea correlation for the Last Interglacial complex. Earth and Planetary Science Letters 171, 123–137

Sánchez Goñi, M.F., 2006. Interactions vegetation-climat au cours des derniers 425 000 ans en Europe occidentale. Le message du pollen des archives marines. Quaternaire 17, 3–25.

Shackleton, N.J., et al., 2000a. revised June 2002. MD95-2042 Oxygen and Carbon Isotope Data. IGBP PAGES/World Data Center A for Paleoclimatology Data Contribution Series #2000-066, NOAA/ NGDC Paleoclimatology Program, Boulder CO, USA.

Shackleton, N.J., Hall, M.A., Vincent, E., 2000b. Phase relationships between millennial scale events 64,000–24,000 years ago. Paleoceanography 15, 565–569.

Shakun, J.D., Carlson, A.E., 2010. A global perspective on Last Glacial Maximum to Holocene climate change. Quaternary Science Reviews 29, 1801-1816. Doi:10.1016/j.quascirev.2010.03.016

Stow, D.A.V., Hernández-Molina, F.J., Alvarez Zarikian, C.A., and the Expedition 339 Scientists (2013). Proceedings of the Integrated Ocean Drilling Program, Volume 339

Thevenon, F., Bard, E., Williamson, D., Beaufort, L., 2004. A biomass burning record from the West Equatorial Pacific over the last 360 ky: methodological, climatic and anthropic implications. Paleogeography, Palaeoclimatology, Palaeoecology 213, 83–99.

Thonicke, K., Prentice, C.I., Hewitt, C., 2005. Modeling Glacial–Interglacial changes in global fire regimes and trace gas emissions. Global Biogeochemical Cycles 19, GB3008.

Tuenter, E., Weber, S. L., Hilgen, F. J., Lourens, L. J., & Ganopolski, A. (2005). Simulation of climate phase lags in response to precession and obliquity forcing and the role of vegetation. *Climate Dynamics*, *24*, 279-295.

Turco, M., Jerez, S., Augusto, S., Tarín-Carrasco, P., Ratola, N., Jiménez-Guerrero, P., Trigo, R.M. 2019. Climate drivers of the 2017 devastating fires in Portugal. Scientific Reports 9, 13886 (2019). https://doi.org/10.1038/s41598-019-50281-2

Tzedakis, P., Channell, J., Hodell, D. *et al.* Determining the natural length of the current interglacial. *Nature Geosci* **5**, 138–141 (2012). https://doi.org/10.1038/ngeo1358

Ulfers, A., Zeeden, C., Voigt, S., Abadi, M. S., & Wonik, T. (2022). Half-precession signals in Lake Ohrid (Balkan) and their spatio-temporal relations to climate records from the European realm. *Quaternary Science Reviews*, *280*, 107413.

Umbanhowar, C.E.J., McGrath, M.J., 1998. Experimental production and analysis of microscopic charcoal from wood, leaves and grasses. The Holocene 8, 341–346.

Vachula, R. S., Sae-Lim, J., & Li, R. (2021). A critical appraisal of charcoal morphometry as a paleofire fuel type proxy. *Quaternary Science Reviews*, *262*, 106979.

Verardo, D.J., Ruddiman, W.F., 1996. Late Pleistocene charcoal in tropical Atlantic deep-sea sediments: climatic and geochemical significance. Geology 24, 855–857.

Whitlock, C. (2001, December). Variations in Holocene fire frequency: a view from the western United States. In *Biology and Environment: Proceedings of the Royal Irish Academy* (pp. 65-77). Royal Irish Academy.

Annex

1. ANOVA tests

1.1. MIS 12 output

```
> summary(AnovaModel.2)
             Df      Sum Sq     Mean Sq F value    Pr(>F)
Climate      2  71739755477 35869877739   10.49 0.0000777 ***
Residuals   93 317897201963  3418249483
---
Signif. codes:  0 '***' 0.001 '**' 0.01 '*' 0.05 '.' 0.1 ' ' 1
1 observation deleted due to missingness


> with(MIS12ANOVA, numSummary(Char.number..nb.g.1., groups = Climate, statistics=c('mean', 'sd')))
                mean       sd data:n
Heath       107657.9 51746.81     37
Med         174778.3 84982.84     11
Semi-desert 160422.7 56357.15     48


> local({
+   .Pairs <- glht(AnovaModel.2, linfct = mcp(Climate = "Tukey"))
+   print(summary(.Pairs)) # pairwise tests
+   print(confint(.Pairs, level=0.95)) # confidence intervals
+   print(cld(.Pairs, level=0.05)) # compact letter display
+   old.oma <- par(oma=c(0, 5, 0, 0))
+   plot(confint(.Pairs))
+   par(old.oma)
+ })


           Simultaneous Tests for General Linear Hypotheses


Multiple Comparisons of Means: Tukey Contrasts
```

Fit: aov(formula = Char.number..nb.g.1. ~ Climate, data = MIS12ANOVA)

Linear Hypotheses:

	Estimate	Std. Error	t value	Pr(>|t|)	
Med - Heath == 0	67120	20078	3.343	0.00319	**
Semi-desert - Heath == 0	52765	12791	4.125	< 0.001	***
Semi-desert - Med == 0	-14356	19544	-0.735	0.73876	

Signif. codes: 0 '***' 0.001 '**' 0.01 '*' 0.05 '.' 0.1 ' ' 1

(Adjusted p values reported -- single-step method)

Simultaneous Confidence Intervals

Multiple Comparisons of Means: Tukey Contrasts

Fit: aov(formula = Char.number..nb.g.1. ~ Climate, data = MIS12ANOVA)

Quantile = 2.3648

95% family-wise confidence level

Linear Hypotheses:

	Estimate	lwr	upr
Med - Heath == 0	67120.4485	19639.4791	114601.4178
Semi-desert - Heath == 0	52764.8086	22517.6805	83011.9366
Semi-desert - Med == 0	-14355.6399	-60573.0076	31861.7279

Heath Med Semi-desert

"a" "b" "b"

> oneway.test(Char.number..nb.g.1. ~ Climate, data = MIS12ANOVA) # Welch test

One-way analysis of means (not assuming equal variances)

data: Char.number..nb.g.1. and Climate

F = 10.897, num df = 2.000, denom df = 25.657, p-value = 0.0003752

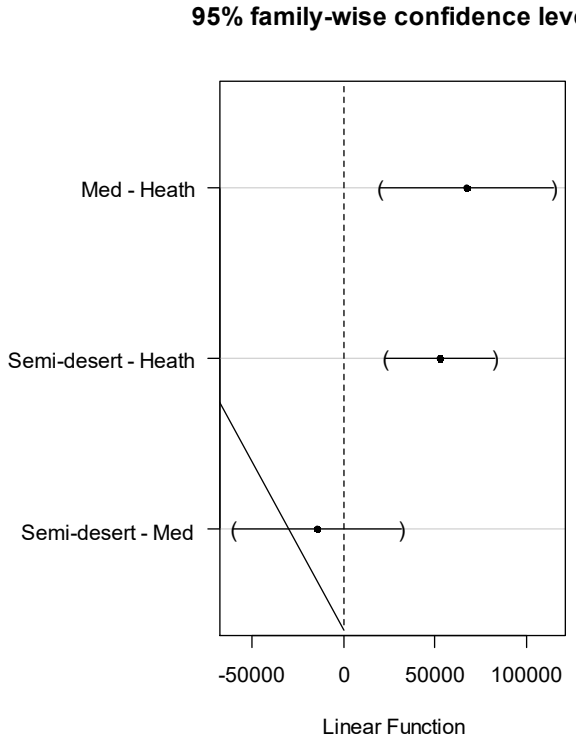

AnovaModel.3 <- aov(elongation ~ Climate, data = MIS12ANOVA)

> summary(AnovaModel.3)

Df Sum Sq Mean Sq F value Pr(>F)

Climate 2 0.234 0.117 0.886 0.416

Residuals 93 12.275 0.132

1 observation deleted due to missingness

```
> with(MIS12ANOVA, numSummary(elongation, groups = Climate, statistics=c('mean', 'sd')))
              mean        sd data:n
Heath       1.923710 0.4749162     37
Med         1.769448 0.4857906     11
Semi-desert 1.851727 0.1954282     48

> local({
+   .Pairs <- glht(AnovaModel.3, linfct = mcp(Climate = "Tukey"))
+   print(summary(.Pairs)) # pairwise tests
+   print(confint(.Pairs, level=0.95)) # confidence intervals
+   print(cld(.Pairs, level=0.05)) # compact letter display
+   old.oma <- par(oma=c(0, 5, 0, 0))
+   plot(confint(.Pairs))
+   par(old.oma)
+ })

           Simultaneous Tests for General Linear Hypotheses

Multiple Comparisons of Means: Tukey Contrasts


Fit: aov(formula = elongation ~ Climate, data = MIS12ANOVA)

Linear Hypotheses:
                       Estimate Std. Error t value Pr(>|t|)
Med - Heath == 0         -0.15426    0.12476  -1.236    0.428
Semi-desert - Heath == 0 -0.07198    0.07948  -0.906    0.632
Semi-desert - Med == 0    0.08228    0.12144   0.678    0.773
(Adjusted p values reported -- single-step method)
```

Simultaneous Confidence Intervals

Multiple Comparisons of Means: Tukey Contrasts

Fit: aov(formula = elongation ~ Climate, data = MIS12ANOVA)

Quantile = 2.3652

95% family-wise confidence level

Linear Hypotheses:

	Estimate	lwr	upr
Med - Heath == 0	-0.15426	-0.44935	0.14082
Semi-desert - Heath == 0	-0.07198	-0.25996	0.11600
Semi-desert - Med == 0	0.08228	-0.20495	0.36951

Heath	Med	Semi-desert
"a"	"a"	"a"

> oneway.test(elongation ~ Climate, data = MIS12ANOVA) # Welch test

One-way analysis of means (not assuming equal variances)

data: elongation and Climate

F = 0.5453, num df = 2.000, denom df = 22.969, p-value = 0.587

1.2.MIS 16 output

```
AnovaModel.5 <- aov(Char.number ~ Climate, data = MIS16ANOVA)

> summary(AnovaModel.5)
             Df      Sum Sq    Mean Sq F value Pr(>F)
Climate      2   5198331217 2599165609   0.449   0.64
Residuals   83 480736781076 5792009411

> with(MIS16ANOVA, numSummary(Char.number, groups = Climate, statistics=c('mean', 'sd')))
               mean       sd data:n
Heath       109301.3 90841.03     20
Med         122050.3 79478.45     13
Semi-desert 100444.2 69079.82     53

> local({
+   .Pairs <- glht(AnovaModel.5, linfct = mcp(Climate = "Tukey"))
+   print(summary(.Pairs)) # pairwise tests
+   print(confint(.Pairs, level=0.95)) # confidence intervals
+   print(cld(.Pairs, level=0.05)) # compact letter display
+   old.oma <- par(oma=c(0, 5, 0, 0))
+   plot(confint(.Pairs))
+   par(old.oma)
+ })

             Simultaneous Tests for General Linear Hypotheses

Multiple Comparisons of Means: Tukey Contrasts


Fit: aov(formula = Char.number ~ Climate, data = MIS16ANOVA)
```

Linear Hypotheses:

	Estimate	Std. Error	t value	Pr(>|t|)
Med - Heath == 0	12749	27114	0.470	0.884
Semi-desert - Heath == 0	-8857	19972	-0.443	0.896
Semi-desert - Med == 0	-21606	23555	-0.917	0.627

(Adjusted p values reported -- single-step method)

Simultaneous Confidence Intervals

Multiple Comparisons of Means: Tukey Contrasts

Fit: aov(formula = Char.number ~ Climate, data = MIS16ANOVA)

Quantile = 2.3768

95% family-wise confidence level

Linear Hypotheses:

	Estimate	lwr	upr
Med - Heath == 0	12748.9979	-51693.3332	77191.3290
Semi-desert - Heath == 0	-8857.1082	-56326.0382	38611.8219
Semi-desert - Med == 0	-21606.1061	-77590.0258	34377.8137

Heath	Med	Semi-desert
"a"	"a"	"a"

> oneway.test(Char.number ~ Climate, data = MIS16ANOVA) # Welch test

One-way analysis of means (not assuming equal variances)

```
data:  Char.number and Climate
F = 0.42516, num df = 2.000, denom df = 26.167, p-value = 0.6581
> AnovaModel.6 <- aov(elongation ~ Climate, data = MIS16ANOVA)

> summary(AnovaModel.6)
             Df Sum Sq Mean Sq F value Pr(>F)
Climate      2  0.824  0.4119   2.846 0.0637 .
Residuals   83 12.011  0.1447
---
Signif. codes:  0 '***' 0.001 '**' 0.01 '*' 0.05 '.' 0.1 ' ' 1

> with(MIS16ANOVA, numSummary(elongation, groups = Climate, statistics=c('mean', 'sd')))
                mean        sd data:n
Heath       2.115550 0.3412774     20
Med         1.793484 0.5084126     13
Semi-desert 1.970693 0.3588495     53

> local({
+   .Pairs <- glht(AnovaModel.6, linfct = mcp(Climate = "Tukey"))
+   print(summary(.Pairs)) # pairwise tests
+   print(confint(.Pairs, level=0.95)) # confidence intervals
+   print(cld(.Pairs, level=0.05)) # compact letter display
+   old.oma <- par(oma=c(0, 5, 0, 0))
+   plot(confint(.Pairs))
+   par(old.oma)
+ })

             Simultaneous Tests for General Linear Hypotheses

Multiple Comparisons of Means: Tukey Contrasts
```

Fit: aov(formula = elongation ~ Climate, data = MIS16ANOVA)

Linear Hypotheses:

	Estimate	Std. Error	t value	Pr(>|t|)	
Med - Heath == 0	-0.32207	0.13553	-2.376	0.0499	*
Semi-desert - Heath == 0	-0.14486	0.09983	-1.451	0.3151	
Semi-desert - Med == 0	0.17721	0.11774	1.505	0.2892	

Signif. codes: 0 '***' 0.001 '**' 0.01 '*' 0.05 '.' 0.1 ' ' 1

(Adjusted p values reported -- single-step method)

Simultaneous Confidence Intervals

Multiple Comparisons of Means: Tukey Contrasts

Fit: aov(formula = elongation ~ Climate, data = MIS16ANOVA)

Quantile = 2.3769

95% family-wise confidence level

Linear Hypotheses:

	Estimate	lwr	upr
Med - Heath == 0	-0.32206568	-0.64419113	0.00005977
Semi-desert - Heath == 0	-0.14485690	-0.38213805	0.09242425
Semi-desert - Med == 0	0.17720878	-0.10263593	0.45705349

Heath Med Semi-desert

"a" "b" "ab"

> oneway.test(elongation ~ Climate, data = MIS16ANOVA) # Welch test

One-way analysis of means (not assuming equal variances)

data: elongation and Climate

F = 2.3314, num df = 2.000, denom df = 26.413, p-value = 0.1168

> with(MIS16ANOVA, cor.test(Char.number, elongation, alternative="two.sided", method="pearson"))

1.3. Pearson's product-moment correlation (additionally for MIS 16)

data: Char.number and elongation

t = -2.365, df = 84, p-value = 0.02033

alternative hypothesis: true correlation is not equal to 0

95 percent confidence interval:

-0.43852183 -0.04010971

sample estimates:

cor

-0.2498616

2. Paired t-test for average pollen percentage comparison between LGP, MIS 12 and MIS 16

data: Semi.desert.12 and semi.desert.LGP

t = -4.7754, df = 91, p-value = 0.000006831

alternative hypothesis: true mean difference is not equal to 0

-12.607003 -5.199985

sample estimates:

mean difference

-8.903494

Paired t-test

data: Semi.desert.12 and Semi.desert.16

t = -0.11376, df = 91, p-value = 0.9097

alternative hypothesis: true mean difference is not equal to 0

95 percent confidence interval:

-3.465943 3.090444

sample estimates:

mean difference

-0.1877496

Paired t-test

data: Semi.desert.16 and semi.desert.LGP

t = -4.2908, df = 91, p-value = 0.00004432

alternative hypothesis: true mean difference is not equal to 0

95 percent confidence interval:

-12.750566 -4.680923

sample estimates:

mean difference

-8.715744

Paired t-test

data: med.forest.12 and med.forest.LGP

t = 3.4541, df = 103, p-value = 0.0008027

alternative hypothesis: true mean difference is not equal to 0

95 percent confidence interval:

1.288477 4.763133

sample estimates:

mean difference

3.025805

Paired t-test

data: med.forest.LGP and med.forest.MIS16

t = -3.7742, df = 91, p-value = 0.0002856

alternative hypothesis: true mean difference is not equal to 0

95 percent confidence interval:

-5.533360 -1.717318

sample estimates:

mean difference

-3.625339

Paired t-test

data: med.forest.MIS16 and med.forest.12

t = 1.8112, df = 91, p-value = 0.07341

alternative hypothesis: true mean difference is not equal to 0

95 percent confidence interval:

-0.1691971 3.6681249

sample estimates:

mean difference

1.749464

3. MIS 12 Charcoal data

crmcd	ge model (Hodell et al. 2022)	EXPEDITI	SITE	HOL	CC	CO	SE	TOP_	BOTT	Serie	Elongation	surf totale	nb total 20	poids sec	Char number (nb.g-1)	Char surface (µm².g-1)	Char mean surface
55.71864407	418.7838136	339	1385	D	7	H	2	14	15	97/5	2.024032	6828.342	56	0.2	315924.636	38522168.98	121.93
55.72762712	422.4354237	339	1385	D	7	H	2	15	16	295/2	2.43249	1497.612	10	0.209	53985.755	8084973.56	149.76
55.73661017	426.0870339	339	1385	D	7	H	2	16	17	97/6	1.728897	5552.546	34	0.214	179262.978	29275470.13	163.31
55.74559322	429.7386441	339	1385	D	7	H	2	17	18	295/3	2.023713	1209.35	8	0.201	44907.553	6788620.36	151.17
55.75457627	431.6581356	339	1385	D	7	H	2	18	19	97/7	1.989008	3585.997	25	0.218	129392.462	18560037.21	143.44
55.76355932	431.909661	339	1385	D	7	H	2	19	20	97/8	1.711304	4236.492	26	0.208	141037.784	22980978.61	162.94
55.77254237	432.1611864	339	1385	D	7	H	2	20	21	missing							
55.78152542	432.4127119	339	1385	D	7	H	2	21	22	missing							
55.79050847	432.6565601	339	1385	D	7	H	2	22	23	98/1	1.698576	2166.323	17	0.217	88392.344	11263902.42	127.43
55.79949153	432.7724547	339	1385	D	7	H	2	23	24	295/6	2.10215	2655.806	8	0.203	44465.114	14761341.85	331.98
55.80847458	432.8883493	339	1385	D	7	H	2	24	25	98/2	1.441168	5716.16	31	0.2	174886.852	32247779.33	184.39
55.81745763	433.004244	339	1385	D	7	H	2	25	26	295/7	2.286467	1059.02	9	0.207	49056.621	5772436.40	117.67
55.82644068	433.1201386	339	1385	D	7	H	2	26	27	98/3	1.877693	3989.623	28	0.199	158756.099	22620605.38	142.49
55.83542373	433.2360332	339	1385	D	7	H	2	27	28	295/9	2.37215	1764.637	10	0.195	57861.655	10210481.73	176.46
55.84440678	433.3519279	339	1385	D	7	H	2	28	29	98/4	1.603316	4746.627	25	0.218	129392.462	24567108.68	189.87
55.85338983	433.4678225	339	1385	D	7	H	2	29	30	295/10	2.679862	1721.224	13	0.209	70181.481	9292159.28	132.40
55.86237288	433.5837171	339	1385	D	7	H	2	30	31	98/5	1.914876	3427.695	34	0.204	188050.379	18958215.41	100.81
55.87135593	433.6996118	339	1385	D	7	H	2	31	32	295/12	3.09888	3064.275	15	0.209	80978.632	16542718.76	204.28
55.88033898	433.8155064	339	1385	D	7	H	2	32	33	98/6	1.720108	5109.975	38	0.205	209148.714	28124862.71	134.47
55.88932203	433.931401	339	1385	D	7	H	2	33	34	296/1	2.115642	3050.521	12	0.199	68038.328	17296027.89	254.21
55.89830508	434.0472956	339	1385	D	7	H	2	34	35	98/7	1.999073	4283.453	33	0.212	175631.957	22797308.56	129.80
55.90728814	434.1631903	339	1385	D	7	H	2	35	36	296/2	2.270529	3663.379	28	0.204	154865.018	20261759.62	130.83
55.91627119	434.2790849	339	1385	D	7	H	2	36	37	98/8	2.008531	9031.742	49	0.206	268382.579	49468618.25	184.32
55.92525424	434.3949795	339	1385	D	7	H	2	37	38	296/3	2.298095	3797.068	37	0.207	201677.218	20696813.24	102.62
55.93423729	434.5108742	339	1385	D	7	H	2	38	39	99/1	2.29123	4584.296	30	0.203	166744.178	25480152.86	152.81
55.94322034	434.6267688	339	1385	D	7	H	2	39	40	99/2	1.860587	5963.349	45	0.208	244103.857	32348365.39	132.52
55.95220339	434.7426634	339	1385	D	7	H	2	40	41	missing							
55.96118644	434.8585581	339	1385	D	7	H	2	41	42	missing							
55.97016949	434.9744527	339	1385	D	7	H	2	42	43	99/3	1.817166	2897.057	35	0.204	193581.272	16023312.60	82.77
55.97915254	435.0903473	339	1385	D	7	H	2	43	44	296/4	2.250122	904.2946	9	0.198	51286.467	5153119.45	100.48
55.98813559	435.206242	339	1385	D	7	H	2	44	45	99/4	1.792573	6687.757	52	0.213	275454.076	35426344.70	128.61
55.99711864	435.3221366	339	1385	D	7	H	2	45	46	298/1	2.072032	2589.318	19	0.197	108821.031	14830119.84	136.28
56.00610169	435.4380312	339	1385	D	7	H	2	46	47	99/5	1.841756	3228.525	34	0.205	187133.060	17769519.66	94.96
56.0420339	435.9016098	339	1385	D	7	H	2	50	51	86/4	2.114872	2876.003	18	0.205	99070.443	15829272.91	159.78
56.08	436.3914286	339	1385	D	7	H	2	54	55	86/5	1.896065	3330.359	23	0.213	121835.457	17641556.94	144.80
56.12	436.9074877	339	1385	D	7	H	2	58	59	86/6	1.5425	72.2158	1	0.203	5558.139	401385.47	72.22
56.16	437.4235468	339	1385	D	7	H	2	62	63	86/7	1.815809	1482.866	11	0.199	62368.467	8407641.34	134.81
56.2	437.9396059	339	1385	D	7	H	2	66	67	86/8	1.682363	1228.582	8	0.202	44685.239	6862434.96	153.57
56.24	438.455665	339	1385	D	7	H	2	70	71	87/1	1.639685	3182.229	26	0.215	136445.856	16700074.35	122.39
56.28	438.9717241	339	1385	D	7	H	2	74	75	87/2	1.852141	2145.833	22	0.208	119339.663	11640137.44	97.54
56.32	439.4877833	339	1385	D	7	H	2	78	79	87/3	1.712865	5997.703	40	0.198	227939.853	34177889.64	149.94
56.36	440.0038424	339	1385	D	7	H	2	82	83	87/4	1.864913	3887.441	24	0.205	132093.925	21396139.64	161.98
56.4	440.5199015	339	1385	D	7	H	2	86	87	87/5	1.841492	2897.316	26	0.215	136445.856	15204873.90	111.44
56.44	441.0359606	339	1385	D	7	H	2	90	91	87/6	1.8809	2992.14	25	0.201	140336.104	16796210.19	119.69
56.48	441.5520197	339	1385	D	7	H	2	94	95	87/7	1.724379	1933.955	19	0.207	103563.977	10541475.22	101.79
56.52	442.0680788	339	1385	D	7	H	2	98	99	87/8	1.70744	1848.125	15	0.2	84622.670	10426216.49	123.21
56.56	442.5841379	339	1385	D	7	H	2	102	103	88/1	2.000682	4002.701	28	0.2	157962.318	22581282.04	142.95
56.6	443.100197	339	1385	D	7	H	2	106	107	88/2	1.573828	9867.63	53	0.215	278139.630	51784507.04	186.18
56.64	443.6162562	339	1385	D	7	H	2	110	111	88/3	1.681046	4529.784	37	0.201	207697.433	25427687.21	122.43
56.68	444.1323153	339	1385	D	7	H	2	114	115	88/4	1.802489	5943.782	38	0.214	200352.740	31338234.45	156.42
56.72	444.6483744	339	1385	D	7	H	2	118	119	88/5	1.903731	5388.381	39	0.226	194707.029	26901429.11	138.16
56.76	445.1644335	339	1385	D	7	H	2	122	123	88/6	1.784117	5531.542	36	0.211	192506.549	29579387.89	153.65
56.8	445.6804926	339	1385	D	7	H	2	126	127	88/7	1.874007	3943.797	27	0.21	145067.435	21189497.87	146.07
56.84	446.1965517	339	1385	D	7	H	2	130	131	88/8	1.587416	3934.568	32	0.211	171116.932	21039725.73	122.96
56.88	446.7126108	339	1385	D	7	H	2	134	135	89/1	1.674691	5561.451	35	0.206	191701.842	30461152.73	158.90
56.92	447.22867	339	1385	D	7	H	2	138	139	89/2	2.149225	3996.42	24	0.2	135396.273	22545848.27	166.52
56.96	447.7447291	339	1385	D	7	H	2	142	143	89/3	2.24959	2337.065	21	0.207	114465.448	12738725.61	111.29
57	448.2607882	339	1385	D	7	H	2	146	147	89/4	1.878292	8781.828	39	0.199	221124.566	49791738.88	225.18
57.09	449.4219212	339	1385	D	7	H	3	150	151	89/6	1.771682	8438.456	56	0.204	309730.036	46672200.27	150.69
57.13	449.9379803	339	1385	D	7	H	3	154	155	89/7	1.702022	6695.328	37	0.226	184722.053	33426344.73	180.95
57.17	450.4540394	339	1385	D	7	H	3	12	13	296/12	2.433323	1049.961	13	201	72.975	5893.90	80.77
57.21	450.9700985	339	1385	D	7	H	3	16	17	297/1	1.6676	1779.161	11	0.209	59384.330	9604932.23	161.74
57.25	451.4861576	339	1385	D	7	H	3	20	21	89/8	2.01615	5675.771	32	0.206	175270.256	31087309.01	177.37
57.29	452.0022167	339	1385	D	7	H	3	24	25	297/2	2.216197	4112.355	34	0.201	190857.101	23084477.33	120.95
57.33	452.5182759	339	1385	D	7	H	3	28	29	90/1	1.890356	1922.99	16	0.209	86377.207	10381406.10	120.19
57.37	453.034335	339	1385	D	7	H	3	32	33	90/2	1.851333	1210.108	12	0.201	67361.330	6792874.79	100.84
57.41	453.5503941	339	1385	D	7	H	3	36	37	90/3	2.06453	2389.81	23	0.2	129754.761	13482139.70	103.90
57.45	454.0664532	339	1385	D	7	H	3	40	41	90/4	1.984747	1856.201	19	0.205	104574.357	10216370.89	97.69
57.49	454.5825123	339	1385	D	7	H	3	44	45	297/3	2.607884	3547.498	25	0.205	137597.838	19525124.42	141.90
57.53	455.0985714	339	1385	D	7	H	3	48	49	90/5	1.569086	752.4519	7	0.201	39294.109	4223846.71	107.49
57.57	455.6146305	339	1385	D	7	H	3	52	53	90/6	1.931467	1228.342	9	0.2	50773.602	6929707.61	136.48
57.61	456.1306897	339	1385	D	7	H	3	56	57	90/7	1.594009	1097.908	11	0.218	56932.683	5682441.82	99.81
57.65	456.6467488	339	1385	D	7	H	3	60	61	90/8	1.69153	819.4964	10	0.2	56415.114	4623198.25	81.95
57.69	457.1628079	339	1385	D	7	H	3	64	65	91/1	1.86956	2318.67	20	0.21	107457.359	12457906.69	115.93
57.73	457.678867	339	1385	D	7	H	3	68	69	91/2	2.086365	2033.829	23	0.211	122990.295	10875704.53	88.43
57.77	458.1949261	339	1385	D	7	H	3	72	73	25/1	1.996553	4548.561	30	0.212	159665.416	24208264.92	151.62
57.81	458.7109852	339	1385	D	7	H	3	76	77	297/4	1.955464	3533.379	22	0.208	119339.663	19166919.31	160.61
57.85	459.2270443	339	1385	D	7	H	3	80	81	25/2	1.798939	2435.794	28	0.209	151160.113	13149817.19	86.99
57.89	459.7431034	339	1385	D	7	H	3	84	85	25/3	2.020561	4698.549	38	0.209	205145.868	25365470.82	123.65
57.93	460.2591626	339	1385	D	7	H	3	88	89	297/5	1.742762	3441.267	21	0.211	112295.487	18401847.52	163.87
57.97	460.7752217	339	1385	D	7	H	3	92	93	25/4	1.935313	2403.72	23	0.206	125975.496	13165646.00	104.51
58.01	461.2912808	339	1385	D	7	H	3	96	97	91/3	1.89968	2070.833	20	0.199	113397.213	11741334.57	103.54
58.05	461.8073399	339	1385	D	7	H	3	100	101	91/4	1.673438	1623.225	16	0.202	89370.477	9066776.77	101.45
58.09	462.323399	339	1385	D	7	H	3	104	105	14/2	1.995144	2598.823	25	0.211	133685.103	13896954.72	103.95
58.13	462.8394581	339	1385	D	7	H	3	108	109	296/5	2.309676	1823.906	21	0.195	121509.475	10553420.81	86.85
58.17	463.3555172	339	1385	D	7	H	3	112	113	296/6	1.65845	1665.123	14	0.2	78981.159	9393811.45	118.94
58.21	463.8715764	339	1385	D	7	H	3	116	117	296/7	1.941076	3052.405	17	0.204	94025.189	16882525.29	179.55
58.25	464.3876355	339	1385	D	7	H	3	120	121	48/7	1.933386	4097.407	35	0.205	192636.973	22551771.05	117.07
58.29	464.9036946	339	1385	D	7	H	3	124	125	296/8	2.019893	3119.544	15	0.207	81761.034	17003811.76	207.97
58.33	465.4197537	339	1385	D	7	H	3	128	129	297/6	2.131684	3877.083	31	0.205	170621.319	21339130.11	125.07
58.37	465.9358128	339	1385	D	7	H	3	132	133	297/7	2.222	3175.23	27	0.209	145761.538	17141718.78	117.60
58.41	466.4518719	339	1385	D	7	H	3	136	137	14/1	4.1485	669.9177	6	0.22	30771.880	3435771.20	111.65
58.45	466.967931	339	1385	D	7	H	3	140	141	296/9	1.503227	5350.905	11	0.201	61747.886	30037007.44	486.45
58.49	467.4839901	339	1385	D	7	H	3	144	145	296/10	1.810517	2289.814	18	0.198	102572.934	13048496.09	127.21
58.53	468.0000493	339	1385	D	7	H	3	148	149	296/11	1.950096	3425.735	26	0.196	149672.750	19720735.38	131.76
58.57	468.5161084	339	1385	D	7	H	4	2	3	48/8	1.973788	10283.98	67	0.22	343619.328	52742902.58	153.49
58.69	470.0642857	339	1385	D	7	H	4	14	15	297/8	1.984921	4831.995	29	0.206	158838.669	26465781.26	166.62
58.73	470.5803448	339	1385	D	7	H	4	18	19	13/8	1.896846	4419.225	28	0.221	142952.324	22562089.24	157.83
58.77	471.0964039	339	1385	D	7	H	4	22	23	missing							
58.97	473.6766995	339	1385	D	7	H	4	42	43	41/4	2.011771	3652.566	34	0.199	192775.263	20709541.42	107.43
59.05	474.7088177	339	1385	D	7	H	4	50	51	13/7	1.89921	929.7725	10	0.222	50824.427	4725515.43	92.98
59.09	475.2248768	339	1385	D	7	H	4	54	55	297/9	2.050223	1331.032	13	0.205	71550.876	7325882.27	102.39
59.25	477.2891133	339	1385	D	7	H	4	70	71	41/7	1.826071	8889.618	58	0.204	320791.823	49167529.79	153.27
59.29	477.8051724	339	1385	D	7	H	4	74	75	297/10	1.871814	797.5793	7	0.196	40296.510	4591380.29	113.94
59.33	478.3212315	339	1385	D	7	H	4	78	79	41/8	1.816435	4758.605	40	0.202	223426.193	26579925.48	118.97
59.37	478.8372906	339	1385	D	7	H	4	82	83	297/11	2.170996	3245.834	27	0.197	154640.413	18590260.48	120.22
59.41	479.3533498	339	1385	D	7	H	4	86	87	13/6	1.912579	1746.914	19	0.207	103563.977	9521964.18	91.94
59.45	479.8694089	339	1385	D	7	H	4	90	91	297/12	2.1459	1807.085	17	0.203	94488.368	10044030.11	106.30
59.49	480.385468	339	1385	D	7	H	4	94	95	42/1	1.741816	5783.552	43	0.208	233254.797	31373053.32	134.50

4. MIS 16 Charcoal data

age		EXPEDITI	SITE	HOLE	COI	CORE	SEC	TOP_D	BOTT	crmcd	Serie	Elongation	surf totale 200ima	nb tot	poids sec	Char number (nb.g-1)	Char surface (µm².g-1	Char mean su
623.90	MIS16	339	1385	D	9	H	3	20	21	76.75	31/2	2.0144623	7808.1188	61	0.207	332494.873	42559991.231	128.002
624.71	MIS16	339	1385	D	9	H	3	24	25	76.79	287/1	2.3443333	2172.2197	21	0.196	120889.529	12504696.039	103.439
625.51	MIS16	339	1385	D	9	H	3	28	29	76.83	287/2	1.8919857	725.2978	7	0.213	37080.356	3842042.985	103.614
626.32	MIS16	339	1385	D	9	H	3	32	33	76.87	287/3	1.71954	466.9609	5	0.202	27928.274	2608282.399	93.392
627.12	MIS16	339	1385	D	9	H	3	36	37	76.91	287/4	2.3510889	1604.8486	9	0.194	52343.920	9333785.166	178.317
627.93	MIS16	339	1385	D	9	H	3	40	41	76.95	31_3	1.8519361	8130.6786	61	0.21	327744.946	43685062.572	133.290
628.73	MIS16	339	1385	D	9	H	3	44	45	76.99	287/5	2.1510143	443.4276	7	0.207	38155.149	2417006.612	63.347
629.54	MIS16	339	1385	D	9	H	3	48	49	77.03	287/6	2.3257625	847.7035	8	0.214	42179.524	4469466.287	105.963
630.34	MIS16	339	1385	D	9	H	3	52	53	77.07	287/7	2.065475	1285.0679	12	0.205	66046.962	7072902.594	107.089
631.15	MIS16	339	1385	D	9	H	3	56	57	77.11	287/8	1.8264818	1051.8924	11	0.197	63001.650	6024632.412	95.627
631.95	MIS16	339	1385	D	9	H	3	60	61	77.15	31_4	1.9685328	6108.1322	58	0.205	319226.984	33618631.420	105.313
632.76	MIS16	339	1385	D	9	H	3	64	65	77.19	287/9	2.2045	512.1103	5	0.202	27928.274	2860471.362	102.422
633.56	MIS16	339	1385	D	9	H	3	68	69	77.23	287/10	2.8247667	1351.6625	6	0.206	32863.173	7403319.758	225.277
634.37	MIS16	339	1385	D	9	H	3	72	73	77.27	287/11	2.1715286	624.5248	7	0.201	39294.109	3505735.080	89.218
635.17	MIS16	339	1385	D	9	H	3	76	77	77.31	287/12	2.5208467	2260.6481	15	0.212	79832.708	12031577.303	150.710
635.98	MIS16	339	1385	D	9	H	3	80	81	77.35	31_5	1.7942537	7440.0007	67	0.201	376100.757	41764028.339	111.045
636.78	MIS16	339	1385	D	9	H	3	84	85	77.39	288/1	2.5525735	7059.1584	49	0.202	273697.086	39430022.097	144.064
637.59	MIS16	339	1385	D	9	H	3	88	89	77.43	288/2	2.6530429	1202.8925	7	0.21	37610.076	6462982.577	171.842
638.39	MIS16	339	1385	D	9	H	3	92	93	77.47	288/3	2.096825	359.9418	4	0.295	15299.014	1376688.647	89.985
639.20	MIS16	339	1385	D	9	H	3	96	97	77.51	288/4	1.7029727	3377.7968	11	0.205	60543.049	18591101.488	307.072
640.00	MIS16	339	1385	D	9	H	3	100	101	77.55	31/6	1.7385169	8653.1764	65	0.207	354297.815	47166176.789	133.126
640.81	MIS16	339	1385	D	9	H	3	104	105	77.59	288/5	1.6951714	856.0639	7	0.206	38340.368	4688829.338	122.295
641.61	MIS16	339	1385	D	9	H	3	108	109	77.63	288/6	2.2513	327.3537	4	0.2	22566.045	1846769.618	81.838
642.42	MIS16	339	1385	D	9	H	3	112	113	77.67	288/7	2.10475	125.7763	2	0.193	11692.252	735304.068	62.888
643.22	MIS16	339	1385	D	9	H	3	116	117	77.71	288/8	2.1410143	736.5506	7	0.201	39294.109	4134585.650	105.222
644.03	MIS16	339	1385	D	9	H	3	120	121	77.75	31/7	1.6809429	5467.4047	49	0.209	264530.198	29516196.875	111.580
644.83	MIS16	339	1385	D	9	H	3	124	125	77.79	288/9	1.7052	1019.8651	8	0.197	45819.382	5841198.527	127.483
645.64	MIS16	339	1385	D	9	H	3	128	129	77.83	288/10	1.52554	705.3794	5	0.207	27253.678	3844836.618	141.076
646.27	MIS16	339	1385	D	9	H	3	132	133	77.87	288/11	2.550225	627.3148	4	0.197	22909.691	3592897.027	156.829
646.89	MIS16	339	1385	D	9	H	3	136	137	77.91	288/12	2.1522333	801.287	6	0.197	34364.536	4589309.355	133.548
647.52	MIS16	339	1385	D	9	H	3	140	141	77.95	31/8	1.8020135	4807.6535	37	0.221	188901.285	24545187.189	129.937
648.14	MIS16	339	1385	D	9	H	3	144	145	77.99	289/1	3.2912	45.0803	1	0.2	5641.511	254321.025	45.080
648.77	MIS16	339	1385	D	9	H	3	148	149	78.03	289/2	2.78265	185.132	2	0.2	11283.023	1044424.281	92.566
649.40	MIS16	339	1385	D	9	H	3	152	153	78.07	289/3	1.9705857	1426.4221	7	0.198	39889.474	8128461.095	203.775
650.02	MIS16	339	1385	D	9	H	4	2	3	78.11	289/4	2.0946667	329.9841	3	0.21	16118.604	1772960.999	109.995
650.65	MIS16	339	1385	D	9	H	4	6	7	78.15	32_1	1.6113207	4320.714	29	0.205	159613.492	23780836.217	148.990
651.28	MIS16	339	1385	D	9	H	4	10	11	78.19	289/5	1.9353	1582.1012	5	0.196	28783.221	9107593.771	316.420
651.90	MIS16	339	1385	D	9	H	4	14	15	78.23	289/6	2.0764	492.6096	4	0.202	22342.619	2751547.184	123.152
652.53	MIS16	339	1385	D	9	H	4	18	19	78.27	289/7	2.8887267	1965.7407	15	0.208	81367.952	10663219.705	131.049
653.15	MIS16	339	1385	D	9	H	4	22	23	78.31	289/8	2.4799875	796.9074	8	0.208	43396.241	4322848.223	99.613
653.78	MIS16	339	1385	D	9	H	4	26	27	78.35	32/2	1.8623212	3846.4779	33	0.202	184326.609	21485097.798	116.560
654.41	MIS16	339	1385	D	9	H	4	30	31	78.39	289/9	1.5888667	748.0806	3	0.209	16195.726	4038569.574	249.360
655.03	MIS16	339	1385	D	9	H	4	34	35	78.43	289/10	2.45329	1630.4011	10	0.194	58159.911	9482398.278	163.040
655.66	MIS16	339	1385	D	9	H	4	38	39	78.47	289/11	2.0037667	886.2655	9	0.2	50773.602	4999876.888	98.474
656.29	MIS16	339	1385	D	9	H	4	42	43	78.51	289/12	2.3831214	1176.044	14	0.21	75220.151	6318729.131	84.003
656.91	MIS16	339	1385	D	9	H	4	46	47	78.55	32/3	1.8173371	4285.526	35	0.216	182826.757	22385966.315	122.444
657.54	MIS16	339	1385	D	9	H	4	50	51	78.59	290/1	1.6635476	2164.4392	21	0.21	112830.227	11629246.037	103.069
658.16	MIS16	339	1385	D	9	H	4	54	55	78.63	290/2	1.7164231	3435.3127	26	0.195	150440.303	19877287.824	132.127
658.79	MIS16	339	1385	D	9	H	4	58	59	78.67	290/3	1.9424667	2014.5061	21	0.2	118471.739	11364859.052	95.929
659.42	MIS16	339	1385	D	9	H	4	62	63	78.71	290/4	1.6298172	2962.5005	29	0.206	158838.669	16226194.398	102.155
660.04	MIS16	339	1385	D	9	H	4	66	67	78.75	32/4	1.7730673	7906.4325	49	0.201	275058.763	44382317.194	161.356
660.67	MIS16	339	1385	D	9	H	4	70	71	78.79	290/5	1.8899063	2182.7983	16	0.192	94025.189	12827376.469	136.425
661.30	MIS16	339	1385	D	9	H	4	74	75	78.83	290/6	2.07078	1149.0864	15	0.203	83372.089	6386782.248	76.606
661.92	MIS16	339	1385	D	9	H	4	78	79	78.87	290/7	1.7362563	4571.1745	32	0.197	183277.526	26181048.608	142.849
662.55	MIS16	339	1385	D	9	H	4	82	83	78.91	290/8	1.6667278	2273.2849	18	0.199	102057.492	12889208.635	126.294
663.17	MIS16	339	1385	D	9	H	4	86	87	78.95	32_5	2.048186	7600.6168	50	0.213	264859.688	40261939.938	152.012
663.80	MIS16	339	1385	D	9	H	4	90	91	78.99	290/9	1.7775452	3260.0364	31	0.209	167355.839	17599552.527	105.162
664.43	MIS16	339	1385	D	9	H	4	94	95	79.03	290/10	2.2476467	2565.5429	15	0.191	88610.126	15155538.659	171.036
665.05	MIS16	339	1385	D	9	H	4	98	99	79.07	290/11	1.7392659	6128.1936	41	0.202	229011.847	34229974.081	149.468
665.68	MIS16	339	1385	D	9	H	4	102	103	79.11	290/12	2.1650778	1752.9958	9	0.212	47899.625	9329760.116	194.777
666.31	MIS16	339	1385	D	9	H	4	106	107	79.15	32_6	1.7279961	13299.1678	77	0.207	419706.642	72490247.581	172.716
666.93	MIS16	339	1385	D	9	H	4	110	111	79.19	291/1	1.7971152	3170.2886	33	0.211	176464.336	16952814.367	96.069
667.56	MIS16	339	1385	D	9	H	4	114	115	79.23	291/2	1.66285	2148.3244	24	0.197	137458.145	12304361.941	89.514
668.18	MIS16	339	1385	D	9	H	4	118	119	79.27	291/3	1.757212	3874.7685	25	0.195	144654.137	22420051.812	154.991
668.81	MIS16	339	1385	D	9	H	4	122	123	79.31	291/4	1.4981364	1376.9184	11	0.196	63323.087	7926429.386	125.174
669.21	MIS16	339	1385	D	9	H	4	126	127	79.35	32/7	1.6767609	3049.6862	23	0.209	124167.236	16463961.098	132.595
669.61	MIS16	339	1385	D	9	H	4	130	131	79.39	291/5	2.2235129	3873.2403	31	0.194	180295.724	22526731.092	124.943
670.01	MIS16	339	1385	D	9	H	4	134	135	79.43	291/6	1.95878	3091.3278	25	0.2	141037.784	17439760.907	123.653
670.40	MIS16	339	1385	D	9	H	4	138	139	79.47	291/7	1.8852792	2542.3417	24	0.196	138159.462	14635356.721	105.931
670.80	MIS16	339	1385	D	9	H	4	142	143	79.51	291/8	1.75317	3958.9899	30	0.206	164315.865	21684161.653	131.966
671.20	MIS16	339	1385	D	9	H	4	146	147	79.55	32/8	1.7007313	4027.148	32	0.204	176988.592	22273726.664	125.848
671.60	MIS16	339	1385	D	9	H	5	0	1	79.59	291/9	1.8597882	1801.0804	17	0.203	94488.368	10010655.705	105.946
672.00	MIS16	339	1385	D	9	H	5	4	5	79.63	291/10	1.7148833	2109.5428	18	0.214	94903.929	11122438.948	117.197
672.40	MIS16	339	1385	D	9	H	5	8	9	79.67	291/11	1.6788962	2865.3132	26	0.295	99443.590	10959116.592	110.204
672.79	MIS16	339	1385	D	9	H	5	12	13	79.71	291/12	1.6334048	2971.8955	21	0.209	113370.085	16044002.133	141.519
673.19	MIS16	339	1385	D	9	H	5	16	17	79.75	33_2	1.7921957	6316.4838	47	0.205	258683.936	34765380.609	134.393
673.59	MIS16	339	1385	D	9	H	5	20	21	79.79	292/1	1.9339258	3687.7802	31	0.198	176653.386	21014801.917	118.961
673.99	MIS16	339	1385	D	9	H	5	24	25	79.83	292/2	2.08878	1618.3046	15	0.202	83784.822	9039290.879	107.887
674.39	MIS16	339	1385	D	9	H	5	28	29	79.87	292/3	1.8829867	1622.4686	15	0.203	83372.089	9017906.444	108.165
674.79	MIS16	339	1385	D	9	H	5	32	33	79.91	292/4	1.6175615	1017.2871	13	0.204	71901.615	5626506.601	78.253
675.18	MIS16	339	1385	D	9	H	5	36	37	79.95	33/1	1.8007643	7137.0375	56	0.213	296642.851	37806270.560	127.447
675.58	MIS16	339	1385	D	9	H	5	40	41	79.99	292/5	1.7157	1110.3395	10	0.204	55308.935	6141169.514	111.034
675.98	MIS16	339	1385	D	9	H	5	44	45	80.03	292/6	2.35026	1064.307	15	0.192	88148.615	6254479.201	70.954
676.38	MIS16	339	1385	D	9	H	5	48	49	80.07	292/7	2.1933133	1977.7933	15	0.197	85911.341	11327658.247	131.853
676.78	MIS16	339	1385	D	9	H	5	52	53	80.11	292/8	1.8351917	2875.7845	24	0.21	128948.831	15451210.410	119.824
677.18	MIS16	339	1385	D	9	H	5	56	57	80.15	33_3	1.7852	3438.5805	38	0.21	204168.983	18475039.009	90.489
677.57	MIS16	339	1385	D	9	H	5	60	61	80.19					not enough sample			
677.97	MIS16	339	1385	D	9	H	5	64	65	80.23	292/9	1.9973	102.9632	1	0.205	5503.914	566700.549	102.963
678.37	MIS16	339	1385	D	9	H	5	68	69	80.27	292/10	1.5975636	2522.9387	22	0.216	114919.676	13178877.168	114.679
678.77	MIS16	339	1385	D	9	H	5	72	73	80.31	292/11	1.9467188	1372.1135	16	0.204	88494.296	7589013.627	85.757
679.17	MIS16	339	1385	D	9	H	5	76	77	80.35	33_4	1.995466	6743.5438	47	0.211	251327.994	36060453.997	143.480
679.57	MIS16	339	1385	D	9	H	5	80	81	80.39	292/12	2.12415	1555.807	18	0.197	103093.609	8910764.332	86.434
679.96	MIS16	339	1385	D	9	H	5	84	85	80.43	293/1	2.0735154	1387.9815	13	0.193	75999.635	8114314.406	106.768
680.36	MIS16	339	1385	D	9	H	5	88	89	80.47	293/2	1.9322077	1254.2436	13	0.202	72613.513	7005771.802	96.480
680.76	MIS16	339	1385	D	9	H	5	92	93	80.51	293/3	2.48042	839.6539	10	0.197	57274.227	4809052.809	83.965
681.16	339		1385	D	10	H	6	96	97	80.55	33/5	1.7451255	7473.5614	55	0.2	310283.125	42162181.551	135.883